Performance evaluation of a variable-speed contra-rotating pump-turbine for low-head pumped hydro energy storage: An experimental study

Energy Conversion and Management: X 26 (2025) 101009

Contents lists available at ScienceDirect

Energy Conversion and Management: X

journal homepage: www.sciencedirect.com/journal/energy-conversion-and-management-x

Performance evaluation of a variable-speed contra-rotating pump-turbine for low-head pumped hydro energy storage: An experimental study

Ruben Ansorena Ruiz [a,*], David Schürenkamp [a], Daan P.K. Truijen [b,c], Justus P. Hoffstaedt [d], Antonio Jarquin Laguna [d], Jonathan Fahlbeck [e], Håkan Nilsson [e], Melvin Joseph [f], Mehrdad Zangeneh [f], Jeroen D.M. De Kooning [b,c], Jonas Oldeweme [g], Heiko Schwarz [g], Nils Goseberg [a,h,*]

[a] Leichtweiß-Institute for Hydraulic Engineering and Water Resources, Technische Universität Braunschweig, Braunschweig, Germany
[b] Department of Electromechanical, Systems & Metal Engineering, Ghent University, Sint-Martens-Latemlaan 2B, 8500 Kortrijk, Belgium
[c] FlandersMake@UGent – Corelab MIRO, Belgium
[d] Faculty of Mechanical, Maritime and Materials Engineering, Department of Maritime and Transport Technology, Delft University of Technology, Mekelweg 2, 2628 CD Delft, the Netherlands
[e] Department of Mechanics and Maritime Sciences, Division of Fluid Dynamics, Chalmers University of Technology, 412 96 Gothenburg, Sweden
[f] Advanced Design Technology Ltd., London, United Kingdom
[g] Institute of Jet Propulsion and Turbomachinery, TU Braunschweig, Braunschweig, Germany
[h] Coastal Research Center, Joint Research Facility of Leibniz University Hannover and Technische Universität Hannover, Hannover, Germany

ARTICLE INFO

Keywords:
Pumped hydro storage
Energy storage
Laboratory tests
Hydraulic machine characterization
Contra-rotating
Pump-turbine

ABSTRACT

Pumped Hydro Energy Storage (PHS) provides over 90% of the global long-duration energy storage capacity, yet many regions lack the steep terrain required for conventional high-head PHS. Low-head pumped hydro energy storage (LH PHS) systems address this gap in flat topographic regions but requires efficient pump-turbine technology for operation at variable low heads. This study investigates the use of a variable-speed contra-rotating pump-turbine (CR RPT) for LH PHS applications, presenting experimental results from a model-scale test rig stablished at Technische Universität Braunschweig. This test rig uses two open water surface tanks to provide head, unlike conventional hydraulic test rigs that use pumps. The CR RPT achieved hydraulic efficiencies over 80% for a wide range of operating conditions, peaking at 86.1% and 88.4% for pump and turbine modes, respectively. Additionally, dimensionless analysis revealed that the CR-RPT occupies a unique place in the market and that it achieves the largest power density among comparable hydraulic machines, facilitating greater power output and thus streamlining mechanical and civil engineering requirements for LH PHS.

Introduction

Pumped hydro energy storage (PHS) is the most widespread form of large scale energy storage. According to the International Hydropower Association over 90 % of the long-duration energy storage in the world corresponds to PHS [1]. PHS grows in importance as more renewable energy sources are connected to the electric grid because of its ability to store energy and release it in-demand, which is not possible for renewable energy technologies such as wind or solar power. Currently operating PHS systems make use of large gross heads (100–800 m) [2,3]. However, flat topography areas such as northern Germany, the Netherlands, and Belgium do not have suitable high-head topography. For those regions, the need for a low-head pumped hydro energy storage (LH PHS) technology concept arises.

LH PHS was first mentioned in the 1980s by the Dutch engineer Luc Lievense as, in the context of the 1973 oil crisis, LH PHS came up as a way of utilizing and storing wind energy [4]. However, the plan was never implemented due to scarce wind power technology development, environmental concerns, and large initial investment costs. In 2007, KEMA Consulting presented a new LH PHS solution which was also not realized due to economic concerns [5,6]. Nowadays, as the share of renewable energies in the EU keeps growing and several offshore wind energy projects are already implemented with more to come in the following years, the feasibility of LH PHS is again being studied. Projects such as DELTA21 [7,8] and ALPHEUS [9] are currently developing

* Corresponding authors.
E-mail addresses: r.ansorena-ruiz@tu-braunschweig.de (R. Ansorena Ruiz), n.goseberg@tu-braunschweig.de (N. Goseberg).

https://doi.org/10.1016/j.ecmx.2025.101009
Received 11 January 2025; Received in revised form 5 April 2025; Accepted 5 April 2025
Available online 9 April 2025

Nomenclature

Abbreviations

E_{nD}	Energy coefficient
h_{dev_i}	vertical distance from the centerline of pipe 1 to each of the pressure transducers *(m)*
h_{pc}	pipe 1 centerline height *(m)*
h_s	spillway height *(m)*
H_P	Net head in pump mode *(m)*
H_T	Net head in turbine mode *(m)*
H_{cf_i}	head correction factor*(m)*
H_i	corrected head *(m)*
$H_{rawdata_i}$	Head in meters as measured in the raw data *(m)*
H_{static_i}	measured head at each pressure transducer when the lower tank is filled up to its maximum level and the butterfly valves are closed *(m)*
H_{ti}	theoretical pressure head *(m)*
n_{ED}	Speed factor
n_{prot}	rotational speed at prototype scale *(rpm)*
P_h	hydraulic power available to the machine *(kW)*
P_{ED}	Power factor
P_m	mechanical power *(kW)*
P_{nD}	Power coefficient
P_{norm}	normalized power
P_{prot}	Power at prototype scale *(MW)*
Q_{ED}	Discharge factor
Q_{nD}	Discharge coefficient
Q_{prot}	Discharge at prototype scale *(m^3/s)*
Ω_s	specific speed for pump mode
Ω_{sp}	power specific speed for turbine mode
η_{norm}	normalized efficiency
λ_L	Geometric scale
τ_h	hydraulic torque *(N•m)*
τ_f	friction torque *(N•m)*.
τ_g	measured torque *(N•m)*
AF	Axial Flux
ALPHEUS	Augmenting Grid Stability Through Low Head Pumped Hydro Energy Utilization and Storage
BEP	Best Efficiency Point
BV1	Butterfly valve 1
CR RPT	Contra rotating reversible pump turbine
DAQ	data acquisition system
LH PHS	Low head pumped hydro storage
LWI	Leichtweiß Institute for Hydraulic Engineering and Water Resources
PAT	Pump As Turbine
PHS	pumped hydro storage
PMSM	Permanent Magnet Synchronous Motor
R0.70	speed ratio 0.70: rotational speed of Runner 2 divided by rotational speed of Runner 1 = 0.70
R0.75	speed ratio 0.75: rotational speed of Runner 2 divided by rotational speed of Runner 1 = 0.75
R0.80	speed ratio 0.80: rotational speed of Runner 2 divided by rotational speed of Runner 1 = 0.80
R0.90	speed ratio 0.90: rotational speed of Runner 2 divided by rotational speed of Runner 1 = 0.90
R1.00	speed ratio 1.00: rotational speed of Runner 2 divided by rotational speed of Runner 1 = 1.00
rad/s	radians per second
Re	Reynolds number
rpm	revolutions per minute
rps	revolutions per second
SI	International System of units
STO	safety torque off
V1	fully open valve
V1/2	half open valve
V1/4	valve opened at one quarter of its capacity
D	diameter *(m)*
E	specific hydraulic energy *(J/kg)*
H	head *(m)*
J	rotational inertia of the drivetrains *(kg/m^2)*
L	Characteristic length *(m)*
P	Power *(W)*
Q	discharge *(l/s)*
T	Runner torque *(N•m)*
g	gravitational acceleration *(m/s^2)*
n	rotational speed *(rpm)*
u	fluid speed *(m/s)*
η	Hydraulic efficiency
μ	dynamic viscosity of water
ρ	water density *(kg/m^3)*
ω	runner rotational speed *(rad/s)*
ω	rotational speed *(rad/s)*

designs and assessing the feasibility of the LH PHS concept.

Existing LH PHS studies consider a closed dike ring where pump-turbines are installed. The dike ring creates a separation between the sea and the inner basin. A recent optimization study of the dam volume by Prasasti et al. [10] resulted in a dike ring diameter of 1.6 km. Due to both safety concerns and dike volume optimization [11], LH PHS designs consider a lower dike with the water level in the inner basin being lower than that of the sea. The gross head used in LH PHS is expected to be between 5 and 30 m [11,12]. LH PHS operates similarly to traditional PHS, when there is excess renewable energy generation the hydraulic machines pump seawater from the inner basin to the sea, lowering the water level in the inner basin and creating a water level gradient between the sea and the inner basin. When electricity is needed, seawater can be turbined into the inner basin, producing electricity and raising its water level [6].

LH PHS cannot make use of existing pump-turbine technology deployed for mountainous regions, as current pump-turbine technologies work efficiently for high head and low discharge conditions [12]. Additionally, LH PHS should make use of machines able to work efficiently under variable low-head and discharge conditions to keep power and storage capacities similar to those currently available in PHS systems [12]. It should be noted that a head variation of a few meters in a LH PHS system working at 5–30 m is much more significant than it is for a high head PHS system working at 100–800 m.

Currently, bulb turbines are used in tidal energy projects around the world, working under low-head and high discharge conditions. Their efficiency is high for turbine mode, while low for pump mode. The La Rance bulb turbine has a maximum efficiency of 92 % in turbine mode, yet only 66 % in pump mode [13]. Other bulb turbines, such as the ones used by the Annapolis tidal power plant, are not used in pump mode. Dixon and Hall [14] show that bulb turbines, typically used in tidal energy plants, work for maximum heads of 20 m and that Francis turbines generally work with heads much larger than 30 m. Kaplan turbines can work efficiently at operating conditions within the range of LH PHS by adjusting the runner blade angle but this can lead to fatigue failure over time [15,16]. A recent study showed similar wide operating conditions when fixing the runner blade angle and running the machine at variable speeds [17]. However, no studies on Kaplan-type pump

performance has been reported in literature. Thus, there exists a lack of knowledge pertaining to efficient pump-turbines for variable low-head conditions that this work is targeting to fill.

Variable-speed contra-rotating pump-turbines have recently been considered for LH PHS [12,18]. Contra-rotating pump-turbines operate using two impellers that rotate in opposite directions. They operate at larger discharge compared to mixed or radial-flow machines. Its main advantage compared with a single runner pump-turbine is that it operates efficiently at a wider range of head and discharge conditions [18]. Computational fluid dynamics studies have been carried out to investigate the use of these type of hydraulic machines for LH PHS [19,20]. However, no experimental data on contra-rotating pump-turbines designed for LH PHS is available in the literature. Considering this, a realistic model-scale test rig was built in the hydraulics laboratory of the Leichtweiß Institute for Hydraulic Engineering and Water Resources (LWI) of Technische Universität Braunschweig (Germany), using two open water tanks. This is a unique feature as the test rigs reported in literature make use of pumps in a closed-loop system to provide head.

This study evaluates steady state data produced using a variable-speed contra-rotating reversible pump-turbine (CR-RPT). The design of the tested model-scale CR-RPT is based on the runner geometry published by Fahlbeck et al. [20] which includes a 276 mm runner that is a 1:22 scale of a prototype runner with a 6 m diameter, 10 MW power output, a design head of 9 m, a design discharge of 130 m^3/s, and a design rotational speed of 50 rpm. While Kaplan turbines are efficient in this operating range, they cannot operate with large discharge to produce 10 MW. The studies from Valero et al. [21] and Reivax [22] examine Kaplan type turbines operating at heads of 12.5 m and 17.5 m with discharges of 50 m^3/s and 31.2 m^3/s, respectively, generating 6 MW and 5 MW.

This study contributes to the literature by, for the first time, providing and analyzing experimental data regarding a variable-speed CR-RPT designed for LH PHS systems. The primary objective of this study is to evaluate the performance of the CR-RPT in the LWI test rig by assessing its efficiency across a wide range of operating conditions and disclosing its characteristics at its best efficiency point (BEP) to discuss its potential use in a LH PHS system. The secondary objective is to compare the CR-RPT performance to that of other available hydraulic machines in the literature.

Section 2 describes the present CR-RPT test setup characteristics and the performance evaluation so that the tests can be replicated. Section 3 shows the results obtained at the laboratory test rig. Section 4 discusses the applicability of the results. Section 5 summarizes the main conclusions of the present work.

Experimental setup and methodology

Test rig description

The CR-RPT performance tests were conducted between February and March of 2024 in the hydraulic laboratory of the LWI at TU Braunschweig, Germany (see Figs. 1 and 2). The setup includes two open surface water tanks acting as upper and lower basins. The lower tank features an adjustable spillway which permits water levels of 1.7 m, 2.2 m and 2.7 m. However, the machine suffers cavitation for spillway heights below 2.7 m in both pump and turbine modes, so the water level of the lower tank is kept at 2.7 m throughout the experiments. The elevated tank is continuously fed with water from the main reservoir of the laboratory and features a spillway, maintaining a constant water surface elevation of 10.5 m. This configuration results in a gross head of 7.8 m. The lower and elevated tanks are connected by two different pipelines, denominated pipe 1 and pipe 2. Both pipes include a butterfly valve to regulate discharge. Pipe 1 entails the CR-RPT and it consists of sections of a standard EN10217-2/10219-1 [23,24] steel pipe of DN500 PN10 that connects, via two conical pipes (DN500 – 277 mm), to a smaller pipe section (277 mm in diameter) containing the CR-RPT. The conical pipe at the intersection of pipe 1 with the lower tank minimizes head loss both in turbine and pump mode by reducing flow velocity. Pipe 2 is composed of sections of (EN10217-2/10219-1) DN 300 PN10 pipe and it is used exclusively to fill in the lower tank during pump mode. In pump mode the water flows from the elevated tank into the lower tank via pipe 2 and then it is pumped back to the elevated tank using the CR-RPT in pipe 1. A detailed description of the test rig used in this study is found in Hoffstaedt et al. [25].

During normal operation, the butterfly valve 1 (BV1) (see Fig. 1) is always open. However, it is used during a specific test run (see Section "Results from the CR-RPT test rig") to modify the head (also affecting the discharge) input to the CR-RPT in turbine mode.

The CR-RPT (see Figs. 3 and 4) consists of two contra-rotating runners of 276 mm in diameter installed inside a transparent pipe made of acrylic glass, allowing for visual access to both runners, with an interior diameter of 277 mm. These runners are mounted on a hub of 124.5 mm in diameter, whose axis is parallel and concentric to that of the outer pipe. The hub contains the runner shafts, as well as the necessary bearings and seals to transfer the torque of the runners with minimal losses. Both of the runner shafts connect perpendicularly to the motor

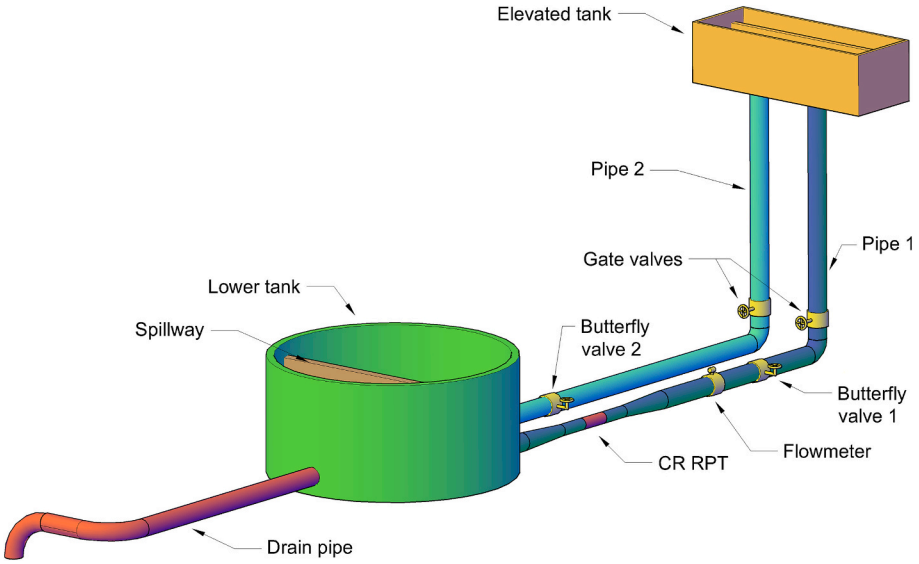

Fig. 1. 3D representation of the hydraulic components of the test rig, indicating where the CR-RPT is positioned.

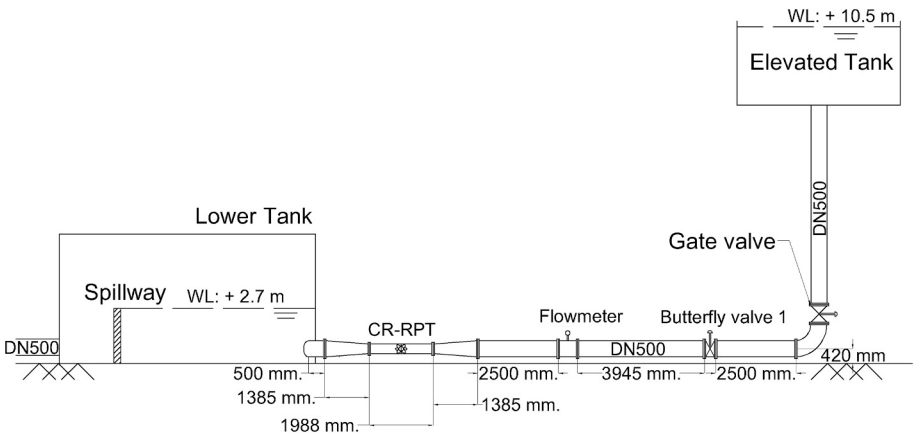

Fig. 2. Schematic drawing of pipe 1 and the tanks.

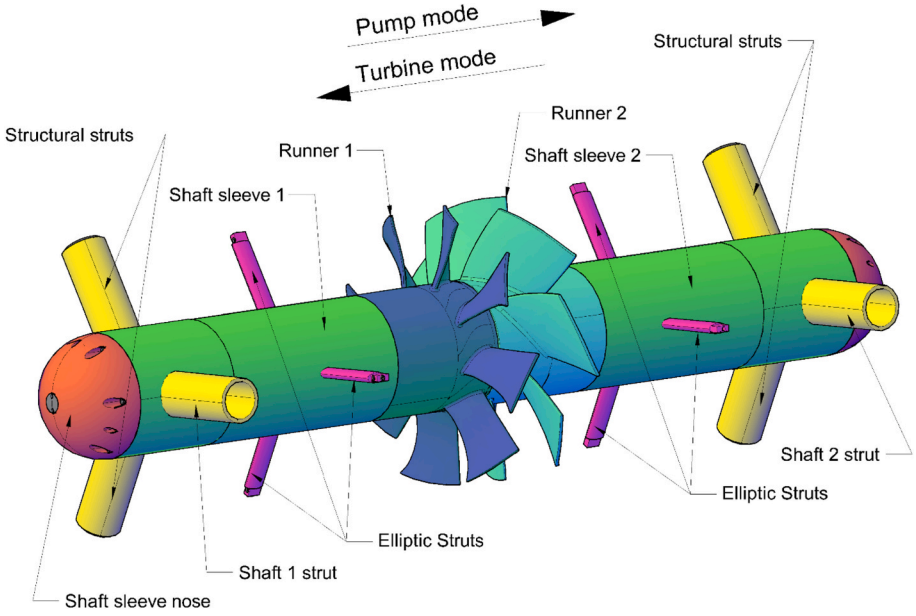

Fig. 3. 3D representation of the CR-RPT including its components. By colors: blue – Runner 1, cyan – Runner 2, yellow – structural and shaft struts (provide stability to the shaft and runner ensemble, and shaft struts also hosts the shaft connecting the bevel gears with the torque meter and thus the electric machines), magenta – elliptical struts (extra support, shaped elliptical to minimize turbulence), green – shaft sleeve (separates bearings, shaft from surrounding fluid), red – shaft sleeve nose. (For interpretation of the references to color in this figure legend, the reader is referred to the web version of this article.)

shafts by the use of bevel gears inside the shaft sleeves, and the motor shafts are positioned inside the shaft 1 and 2 struts seen in Fig. 3. Appendix A shows a mechanical drawing of the arrangement. This power take-off was chosen to minimize interference with the water flow surrounding the runners. The CR-RPT includes a lubricant oil feeder that circulates the lubricant oil within the hub of the machine. This lubricant oil flows through all bearings, ensuring low friction forces.

Each runner is driven by a tailor-made axial flux (AF) permanent magnet synchronous machine (PMSM) [26], coupled to ABB drives (ACS880). This allows to control the speed of each of the runners individually, increasing the operating range of the machine. Fig. 4 shows a photograph of the CR-RPT alongside the electric machines and Fig. 5 presents a close-up of the runners at rest.

Operating procedure

The test rig operates in both turbine and pump mode, with a maximum torque limitation of 200 N•m imposed by the bevel gears. The drives are programmed to limit the torque to 200 N•m.

To limit the maximum torque during turbine mode start-up, the BV1 is slowly opened while monitoring the measured torque. When the measured torque is between 100–150 N•m, the machine is accelerated until $n_1 = 500$ rpm, $n_2 = 400$ rpm (n_1 and n_2 represents the rotational speed of Runner 1 and Runner 2) and the BV1 is fully opened. Steady-state experiments are then carried out at various speed ratios, specifically $n_2/n_1 = 1.00$, 0.90, 0.80, 0.75 and 0.70, denoted as R1.00, R0.90, R0.80, R0.75, R0.70 throughout the manuscript. For each speed ratio, the machine is accelerated from $n_1 = 500$ rpm up to 1200 rpm (1250 rpm for R0.75) in steps of 100 rpm. Each speed setpoint is maintained for 60 s allowing the test rig to achieve steady-state conditions. After reaching the maximum speed, the machine is decelerated again in steps of 100 rpm down to $n_1 = 500$ rpm. This procedure allows data evaluation during both acceleration and deceleration (see Section "Accelerated and decelerated setpoints"). The minimum speed of 500 rpm is chosen as flow separation is observed through the acrylic glass at lower speeds. This lower speeds are in the low efficiency range, being irrelevant for the objectives of this study.

For pump mode start-up, the water level at the lower tank must be at

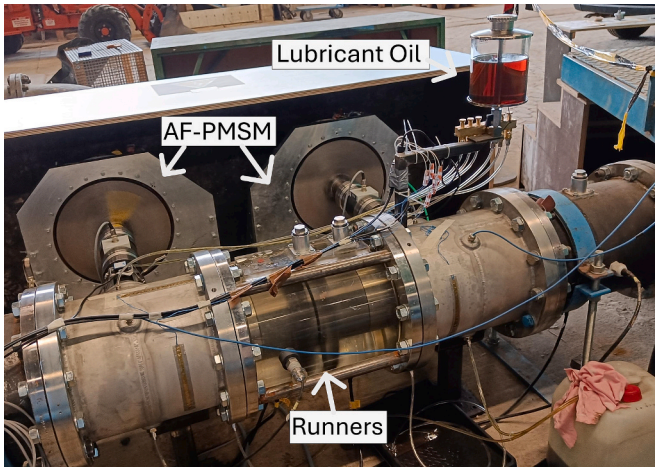

Fig. 4. Photo showing the CR-RPT in operation, with runners visible through the acrylic pipe. The AF PMSM and the lubricant oil system are included in the photo.

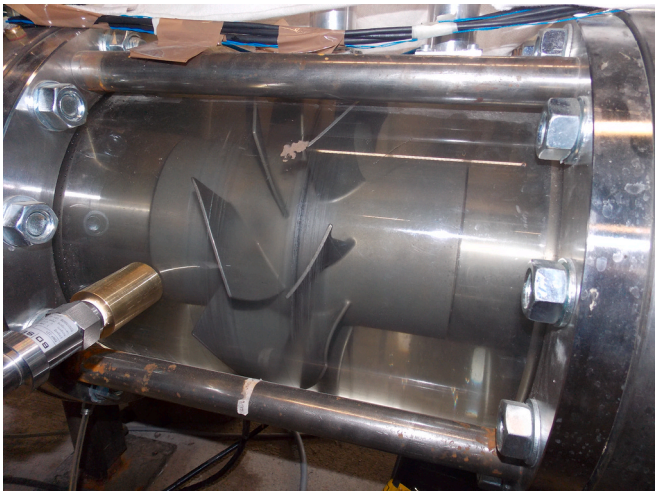

Fig. 5. Detail of the CR-RPT runners seen thought the acrylic glass in a static position at the test rig.

a constant 2.7 m, which is ensured when the pipe 2 feeds water into the lower tank. Then, while the BV1 is closed, the machine is accelerated following a startup sequence developed to limit the maximum torque below 200 N•m [19]. To ensure this the runners are accelerated to $n_1 = n_2 = 700$ rpm and then Runner 1 is accelerated to 1250 rpm while simultaneously opening the BV1. After approximately 3 s, when Runner 1 reaches its speed setpoint and the BV1 is fully opened, Runner 2 is accelerated to 1125 rpm. Once both runners reach the target speeds, the machine is pumping water. During pump mode, setpoints are recorded every 50 rpm for 30 s each. The lower recording time is due to the CR-RPT being subjected to higher torques. As for turbine mode, data is recorded for both accelerating and decelerating setpoints. The maximum speed setpoint in pump mode is limited because cavitation was observed through the acrylic glass in the laboratory.

Data acquisition and measurement

The data acquisition system (DAQ) for the test rig includes 12 pressure transducers, 2 torque transducers, one flowmeter, and 2 encoders, as shown in Fig. 6. It is composed of two parts. First, the Q.bloxx XL A108 from Gantner Instruments GmbH [27] collects data from the flowmeter, torque transducers and pressure transducers. This device is connected to a PC, where data visualization, recording and output are facilitated by the software GI.Bench v1.13 [28]. Second, a MicroLabBox [29] controller inputs data from the encoders into a separate PC which operates the AF PMSM machines. Data recording, visualization, and output is performed using the software ControlDesk v7.1 [30]. To synchronize data acquisition with MicroLabBox and Q.bloxx, an electric signal is sent simultaneously to both systems to trigger data recording. A schematic overview showing the interconnectivity of all data acquisition components is shown in Fig. 7. Table 1 lists all data acquisition elements including their accuracy, measuring range, model and manufacturer.

Data processing and analysis

The raw data is refined in two different steps before evaluating the CR-RPT performance.:

- Pressure transducer calibration
- Torque friction characterization

After refinement, the refined data is used to calculate the performance characterization parameters. Both data refinement and characterization analysis are conducted using Python v3.9.

Pressure transducer calibration

At the beginning of each test day, the lower tank is filled up to its maximum level and the butterfly valves of both pipe 1 and pipe 2 are closed. Thus, the theoretical pressure head (H_{ti}) for each transducer (i = 1, 2 …12) is calculated as

$$H_{t_i} = h_s - h_{pc} - h_{dev_i} \tag{1}$$

here, h_s is the spillway height (m), h_{pc} is the centerline height of pipe 1 (m) and h_{dev_i} is the vertical distance from the centerline of pipe 1 to each of the pressure transducers (m). Thus, a head correction factor (H_{cf_i}) can be calculated as

$$H_{cf_i} = H_{t_i} - H_{static_i} \tag{2}$$

here, $H_{static\,i}$ (m) is the measured head at each pressure transducer when the lower tank is filled up to its maximum level and the butterfly valves are closed. Finally, the corrected head (H_i) is calculated by adding the correction factor to the raw data (H_{raw_i}) as

$$H_i = H_{raw_i} + H_{cf_i} \tag{3}$$

Torque friction characterization

Due to the positions of the torque transducers, it is necessary to characterize the friction between them and the runners. The friction characterization is performed running the machine in dry conditions, i. e. without any water in the pipe system. As the friction depends on the rotational speed, the torque is recorded for a range of different runner speeds. Then, assuming that both the hydraulic torque and drag are zero and that the system is at constant speed, from

$$J_{1,2}\frac{d\omega_{1,2}}{dt} = \tau_{h1,2} - \tau_{g1,2} - \tau_{f1,2}(\omega_{1,2}) \tag{4}$$

it is deducted that the measured torque is equal to the friction torque. In Eq. (4), subscripts 1 and 2 refer to Runner 1 and Runner 2, respectively, J is the rotational inertia of the drivetrains (kg/m^2), ω is the runner rotational speed (rad/s), τ_h is the hydraulic torque (N•m), τ_g is the measured torque (N•m) and τ_f is the friction torque (N•m).

Thus, to obtain the torque at the runners, the friction torque is added to the measured torque as

$$\tau_{h1,2} = \tau_{g1,2} + \tau_{f1,2} \tag{5}$$

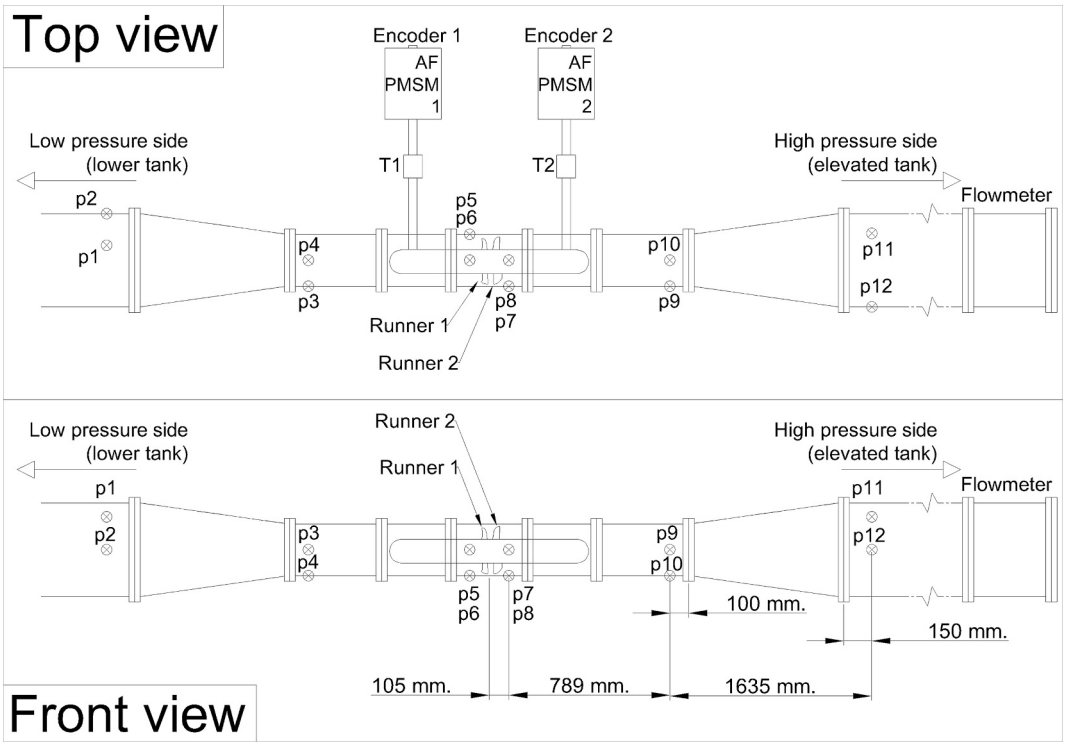

Fig. 6. Distribution of pressure transducers (p1 to p12), torque transducers (T1 and T2) flowmeter, and encoders in the test rig. Dimensions are given from the center point between both runners. The probe distribution is symmetrical respecting the center point between both runners. Drawing not to scale.

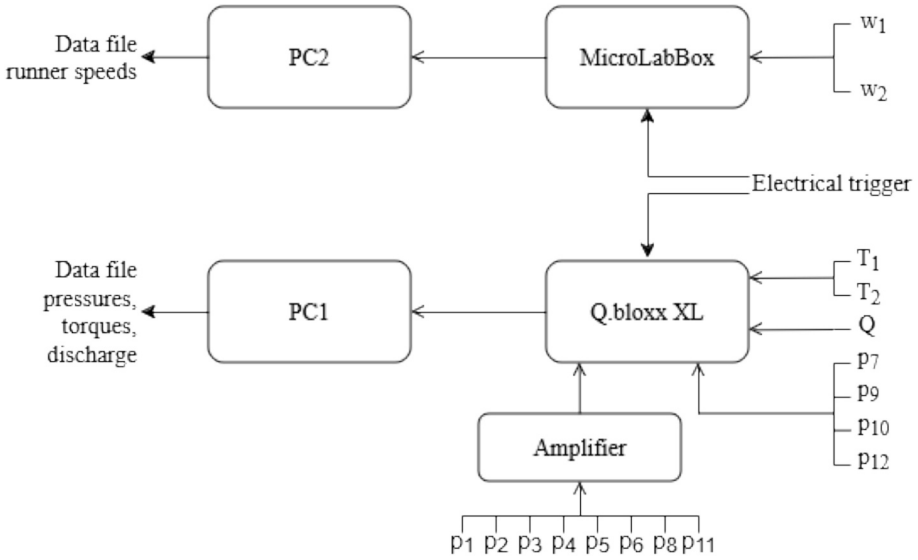

Fig. 7. Diagram of all data acquisition equipment used in the test rig.

Table 1
List of hardware used for data acquisition.

Data Acquisition Parameter	Accuracy of measurement	Measuring range	Model	Manufacturer
p1 – p6	±0.1 %	−0.5 to +0.350 bar	PDCR 1830	Druck Limited
p7, p9, p10, p12	±0.25 %	0 to +2.4 bar	DMP 321	BD|Sensors GmbH
p8, p11	±0.1 %	−0.5 to +5 bar	PDCR 830	Druck Limited
T1, T2	±0.5 %	−500 to +500 N•M	T22	Hottinger Baldwin Messtechnik GmbH
ω_1, ω_2	±0.015 %	−0 to 9000 rpm	DBS60	SICK AG
Flowmeter	±0.312 %	0 to 600 l/s	Optiflux 2000	KROHNE Messtechnik GmbH
Universal Measurement Module (DAQ)	±0.040 %	–	Q.bloxx XL A108	Gantner Instruments GmbH
Controller (DAQ)	–	–	Q.Station X	Gantner Instruments GmbH
MicroLabBox	±0.0015 %	–	MicroLabBox	dSpace GmbH

Performance characterization

The refined data is used to assess the performance of the CR-RPT. First, the steady state setpoint data is identified and then time-averaged. During turbine mode, the data is averaged in intervals of 40 s duration, while during pump mode, it is averaged in 25 s intervals.

The machine performance is first presented by plotting power and efficiency as a function of discharge and by indicating the main parameters at BEP. Second, dimensionless coefficients and factors are calculated, plotted and the parameters at BEP are indicated.

The hydraulic power (P_h, in W) available to the machine during turbine mode and generated by the machine during pump mode is calculated as

$$P_h = \rho \bullet g \bullet H_{T,P} \bullet Q \tag{6}$$

here, ρ is the density of the water (998 kg/m^3), g is the gravitational acceleration (9.81 m/s^2), $H_{T,P}$ is the net head (m) (H_T for turbine and H_P for pump) and Q is the discharge (m^3/s).

The mechanical power (P_{m_i}, in W) of each runner ($i = 1, 2$) is calculated as

$$P_{m_i} = \omega_i \bullet \tau_{h1,2} \tag{7}$$

here, ω is the runner rotational speed (rad/s) and τ_h is the hydraulic torque (N•m). The total mechanical power (P_m) of the machine will be the sum of the mechanical power produced or generated by each runner ($P_m = P_{m1} + P_{m2}$).

When the hydraulic and mechanical power are calculated, the hydraulic efficiency is calculated for turbine (η_T) and pump mode (η_P) as

$$\eta_T = \frac{P_m}{P_h} \tag{8}$$

$$\eta_P = \frac{P_h}{P_m} \tag{9}$$

For the remainder of this study, the term "efficiency" is used instead of "hydraulic efficiency" as this is the only efficiency evaluated.

Dimensionless parameters for pump-turbine performance

To provide a broader perspective on the performance of the CR-RPT presented in this study, this Section compiles dimensionless coefficients defined in the IEC 60193 [31] at the BEP for multiple hydraulic machines reported in the literature. These dimensionless coefficients facilitate comparison of hydraulic machine performance across different sizes.

The dimensionless coefficients, namely, the discharge coefficient (Q_{nD}), energy coefficient (E_{nD}), and power coefficient (P_{nD}) are defined as

$$Q_{nD} = \frac{Q}{\omega \bullet D^3} \tag{10}$$

$$E_{nD} = \frac{E}{\omega^2 \bullet D^2} \tag{11}$$

$$P_{nD} = \frac{P_m}{\rho \bullet \omega^3 \bullet D^5} \tag{12}$$

For Eq. (10) to Eq. (12), Q is the discharge (m^3/s), D is the diameter (m), P is the power (W), E is the specific hydraulic energy, which in the case of this test rig is $E = g \bullet H$ (J/kg), ρ is the density of the water (kg/m^3) and ω is the rotational speed of Runner 1 (rad/s).

Furthermore, the specific speed (Ω_s) is used for pump mode and the power specific speed for turbine mode (Ω_{sp}) [32]. They are defined as

$$\Omega_s = \frac{\omega \bullet Q^{0.5}}{E^{0.75}} = \frac{{Q_{nD}}^{0.5}}{{E_{nD}}^{0.75}} \tag{13}$$

$$\Omega_{sp} = \frac{\omega \bullet \left(\frac{P}{\rho}\right)^{0.5}}{E^{0.75}} = \frac{{P_{nD}}^{0.5}}{{E_{nD}}^{1.25}} \tag{14}$$

Some publications [33–35] use dimensionless coefficients as described in Eq. (10) to Eq. (14). However, the units used for the rotational speed varies between 'rad/s' and 'rps'. IEC Section "1.3.2 Units" states "The international System of Units (SI, see ISO 31–3) has been used throughout this standard." [31], thus 'rad/s' should be used. Note that only using the adequate rotational speed unit (rad/s) results in dimensionless coefficients.

Note that several publications use dimensionless factors rather than dimensionless coefficients to evaluate performance, but these factors can be converted into coefficients and vice versa in the following manner

$$Q_{nD} = \frac{Q_{ED}}{n_{ED}} \tag{15}$$

$$P_{nD} = \frac{P_{ED}}{{n_{ED}}^3} \tag{16}$$

$$E_{nD} = \frac{1}{{n_{ED}}^2} \tag{17}$$

The dimensionless coefficients compiled from the literature are summarized in Table 2. Note that the larger the dimensionless flow, head or power coefficient of a hydraulic machine, the larger the discharge, net head and power generated or consumed at the BEP. Table 2 is used in Section "Comparison of CR-RPT with other hydraulic machines from literature" to compare the CR-RPT performance to that of other hydraulic machines reported in the literature.

Note that dimensionless coefficient formulations are developed for single-runner hydraulic machines, while the CR-RPT has two runners. This study uses the rotational speed of Runner 1 to calculate the dimensionless coefficients. The rotational speed of Runner 2 is represented by the speed ratio.

Uncertainty and error analysis

The following aspects are considered in this study to assess the measurement errors given by:

- Precision of the data acquisition equipment
- Sensitivity analysis of time averaging
- Data differences between accelerated and decelerated setpoints
- Repeatability of the tests

All the relevant theory and methodology used to assess uncertainty is presented in Appendix B. This Section contains the results from the Appendix B.

Precision of the data acquisition equipment

All equipment used in the laboratory has specific errors associated with measuring physical properties. This uncertainty is shown in Table 1. To calculate the error of a parameter calculated from different physical properties, classical error propagation equations are used (see Eq. (B.1) and Eq. (B.2)). Table 3 presents the results from the error propagation.

Accelerated and decelerated setpoints

The differences between reaching a setpoint by accelerating and

Table 2
Performance of hydraulic machines reviewed from the literature in terms of the dimensionless coefficients using standardized units.

–	Turbine mode					Pump mode				
type of pump/turbine	Q_{nD}	E_{nD}	P_{nD}	Ω_{sp}	η	Q_{nD}	E_{nD}	P_{nD}	Ω_s	η
Vaneless centrifugal pump as turbine [33]	0.012	0.24	2.00E-03	0.266	61.5 %	0.017	0.27	2.70E-03	0.35	70 %
centrifugal pump as turbine [34]	0.014	0.486	9.84E-03	0.244	72.5 %	0.01	0.286	7.58E-03	0.26	77 %
centrifugal pump as turbine [35]	0.015	0.583	13E-03	0.224	76.5 %	–	–	–	–	–
Bulb [36]	0.183	0.020	2.40E-03	6.498	86 %	0.067	0.011	1.45E-3	7.77	66 %
Bulb [37]	0.177	0.034	4.90E-03	4.782	89.1 %	–	–	–	–	–
Porjus U9 Kaplan [38]	0.079	0.057	4.52E-03	2.42	–	–	–	–	–	–
Propeller 1 [39]	0.074	0.133	4.88E-3	0.870	73.9 %	–	–	–	–	–
Propeller 2 [39]	0.089	0.099	6.60E-03	1.458	74.5 %	–	–	–	–	–
Propeller 3 [39]	0.099	0.062	4.40E-3	2.141	70.3 %	–	–	–	–	–
Propeller 4 [39]	0.070	0.027	1.29E-3	3.286	68.2 %	–	–	–	–	–
Propeller ultra-low head pump [40]	–	–	–	–	–	0.064	0.020	0.002	5.95	67 %
Bulb [41]	0.101	0.028	–	–	91.7 %	–	–	–	–	–
counter-rotating pump-turbine [42]	0.074	0.110	7.15E-03	1.33	79 %	0.055	0.053	3.96E-03	2.13	75 %
Propeller [43]	0.093	0.075	4.71E-03	1.74	63.8 %	–	–	–	–	–
Francis [44]	0.134	0.785	98.6E-03	0.42	93 %	–	–	–	–	–

Table 3
Maximum relative errors for post-processed parameters.

Parameter	Maximum relative error
P_h	0.33 %
P_{m1}	0.50 %
P_{m2}	0.50 %
P_m	0.50 %
η	0.60 %

decelerating the machine are insignificant for turbine mode after analyzing 34 different setpoints. This is demonstrated in Table B.1 as the maximum relative error is 1.01 % and most of the error values are under 0.3 %. The pump mode, having analyzed 13 data points, shows a higher relative error, having maximum error values of 5 % and 3 % for T_1 and T_2 which propagate to similar relative error for the mechanical power of each runner. This could be explained by the water level reduction happening in the lower tank for large discharge (>330 l/s) setpoints during pump mode as is explained in Appendix B. Additionally, cavitation and/or flow separation at high speeds during pump mode may be present, which could also influence the measured data. In any case, the major differences appear for the measured torque values at each runner. When looking at the total machine mechanical power and efficiency, the errors for 95 % of the pump setpoints in accelerated versus decelerated modes are lower than 2 %.

Sensitivity analysis of time averaging

The data points of the performance curves are obtained from averaging the refined data over a specific time interval over which a setpoint is in steady-state. For the turbine mode, the standard averaging time was 40 s whereas for pump mode it was 25 s.

To assess the influence of averaging time on machine performance, different averaging times were used. For turbine mode, the standard 40 s time average was compared to 30 and 20 s intervals, and for pump mode, the standard 25 s time average was compared to 20 and 15 s time interval. No significant errors are identified when modifying the averaging time in turbine mode. The maximum relative errors are found for the mechanical power of Runner 1, at 0.81 % and 1.03 % for averaging times of 30 and 20 s, respectively. Pump mode showed relative errors for mechanical power of Runner 1 of 2.67 % and 1.98 % for averaging times of 20 and 15 s, respectively. The total mechanical power relative error is 0.78 % for a 15 s time interval. The relative error for efficiency is 0.91 %, happening for averaging time of 20 s. This confirms that using different averaging interval has minimal influence on the results presented in this study, also indicating that the averaged data is in a steady state, as it is practically uniform over time.

Repeatability of the tests

Turbine mode shows a good match between same setpoints recorded on multiple testing days. The most significant errors are in torque of Runner 1 and Runner 2 and therefore translated to the power of the individual runners. The maximum relative error of Runner 1 power is 3.09 %. When assessing total power of the machine the differences between setpoints are negligible (maximum relative error 0.97 %), as well as for efficiency (maximum relative error 0.34 %).

For pump mode, larger errors are found, the relative errors for the power of Runner 2 and total mechanical power are 25.57 %, and 8.35 % respectively. The larger errors happen for high speed points, indicating that these may be affected by cavitation and flow separation, which affect the data by not being fully steady-state. Therefore, different test runs give different average values. The lower speed setpoints show similar data regardless of the testing day (maximum error 1.23 %). The efficiency values show a maximum error of 0.93 % for pump mode.

When assessing performance of same setpoints recorded in different testing days, it shows low relative errors between total power and efficiency values. However, when analyzing the power produced by each runner the error is more significant.

Results

This Section first presents the analysis of post-processed data from the CR-RPT model tests for turbine and pump mode. Next, the normalized results using dimensionless coefficients are presented. Finally, the CR-RPT is compared to other hydraulic machines from the literature. The data generated in the test rig is publicly available here: https://doi.org/10.24355/dbbs.084-202412181712-0.

As a preliminary note, and according to Dixon and Hall [32], the Reynolds number should be large enough for the dimensionless coefficients to be applicable. There are two ways of defining the Reynolds number. The first one reads

$$Re = \frac{\rho \bullet u \bullet L}{\mu} \tag{18}$$

where, $\rho = 998$ kg/m^3 (assumed for water at 20 °C), u the water speed (min: 4.3 m/s (208 l/s) – max: 8.0 m/s (380 l/s)), L is the characteristic length which for a pipe means the hydraulic diameter ($D_{shroud} - D_{hub} = 0.1515$ m), and μ is the dynamic viscosity of the water used in the lab (0.00114 kg/m/s, assumed for water at 20 °C). Thus, considering that the relative roughness is around 0.007, the Reynolds number is between $5.8 \bullet 10^5$ and 10^6, confirming that the fluid is turbulent for all tested

setpoints and thus viscous scale effects can be neglected.

The second way of defining the Reynolds number according to Dixon and Hall [32] is

$$Re_2 = \frac{\rho \bullet \omega \bullet D^2}{\mu} \tag{19}$$

where ρ is the density of the water used in the lab (998 kg/m^3), ω is the rotational speed of the machine (min: 350 rpm = 36.65 rad/s, max: 1250 rpm = 131 rad/s), D is the diameter of the runner and μ is the dynamic viscosity of the water used in the lab (0.00114 kg/m/s). Thus, resulting in a Re_2 range from $2.4 \bullet 10^6$ to $8.7 \bullet 10^6$ which is always larger than the lower limit $2 \bullet 10^5$ [32].

Results from the CR-RPT test rig

Fig. 8 shows the CR-RPT efficiency vs. discharge curves for multiple speed ratios, indicating that the machine works efficiently for a large range of discharges in turbine mode. The BEP is reached at $n_1 = 800$ rpm and $n_2 = 720$ rpm (R0.9) with an efficiency of 86.1 %, with the other measurements summarized in Table 4.

The speed ratio R0.9 is not the most efficient for all conditions. At discharges under BEP (289 l/s), the smaller the speed ratios the larger the efficiency, while for discharges over BEP the efficiency increases with the speed ratio. The overall efficiency of the CR-RPT is depicted by the dashed black line in Fig. 8, indicating that efficiencies larger than 80 % are reached within the discharge range of 91 % to 116 % of the BEP (289 l/s). This efficient range is beneficial for a LH PHS system operating under variable discharge conditions.

Fig. 9 shows the relationship between total mechanical power (P_m) and discharge. The advantages of using multiple speed ratios are less pronounced than for the efficiency curve. Specifically, R0.75, R0.80, R0.90 and R1.00 show a similar power for discharge values above the BEP (289 l/s), while only R0.70 operates at lower power levels. For discharges below 289 l/s, power values vary for each speed ratio with R0.70, R0.75 and R0.80 yielding similar power outputs whereas R0.90 and R1.00 yield lower power. Thus at power outputs below BEP, R0.90 and R1.00 should be avoided during operation. The maximum power of 15.4 kW happens at $n_1 = 1000$ rpm and $n_2 = 800$ rpm (R0.80) with an 84.6 % efficiency, while at least 90 % of the maximum power (13.9 kW) is available from 94 % up to 121 % of the discharge at BEP. Additionally, the machine works at efficiencies higher than 80 % while its power output ranges from 13.0 kW to its maximum of 15.4 kW, indicating that the power remains high for a large range of discharge values.

In a LH-PHS system, the power setpoint may vary according to grid demand. Figs. 8 and 9 showed that the CR-RPT operates efficiently over a large range of power outputs, and that for every power setpoint there is a corresponding speed setpoint and a speed ratio that deliver the desired power efficiently. This enables the CR-RPT to adapt to the fluctuating grid demand while operating at high efficiency. This adaptability can be further enlarged by the use of multiple CR-RPT units, as demonstrated by Prasasti et al. [10].

Fig. 10 presents the power and efficiency for the CR-RPT in pump mode. The studied discharge range does not reveal a clear maximum efficiency for all speed ratios. While there is a maximum for R0.75 and R0.80, additional data would be needed to confirm the reduction in efficiency for higher discharge values. Higher runner rotational speeds necessary to reach higher discharge could not be achieved due to cavitation. Nonetheless, significant efficiency values are achieved in pump mode, peaking at 88.8 % for R0.80, with all speed ratios exceeding 86 % efficiency. Furthermore, the efficiency remains above 80 % across a wide discharge range, from 225 l/s (67 % of BEP) to the BEP at 335 l/s. Table 5 includes a summary of the parameters at BEP for pump mode.

An additional test campaign is performed for turbine mode in which the net head is reduced using the BV1. Similarly to the approach used in Kanemoto et al. [42], the valve position is given as a percentage of the opened area (V1 = 100 %, V1/2 = 50 % and V1/4 = 25 %). This test was conducted for R0.75. Figs. 11 and 12 plot the net head versus discharge. Fig. 11 indicates the normalized efficiency, given by

$$\eta_{norm} = \frac{\eta}{\eta_{max}} \tag{20}$$

for each operation point, which is used to evaluate the efficiency reduction from the maximum when decreasing the net head input. Fig. 12 indicates the normalized power, given by

$$P_{norm} = \frac{P}{P_{max}} \tag{21}$$

for each operation point, used to evaluate the power reduction from the maximum when reducing the net head input.

Fig. 11 demonstrates that the overall maximum efficiency occurs when the valve is fully opened, granting maximum head, consistent with the contra-rotating tests performed by Kanemoto et al. [42]. The maximum efficiency for the V1 and V1/2 curves happen for medium discharge values. In contrast, for the V1/4 curve, which operates under significant lower net head, the maximum efficiency happens at lower discharge values. Nonetheless, the maximum efficiency at V1/4 is 97 % of that at V1. Fig. 12 shows similar behavior, with the difference that the drop in power is larger than the drop in efficiency due to the large drop in net head.

Notably, the butterfly valve provides additional operational flexi-

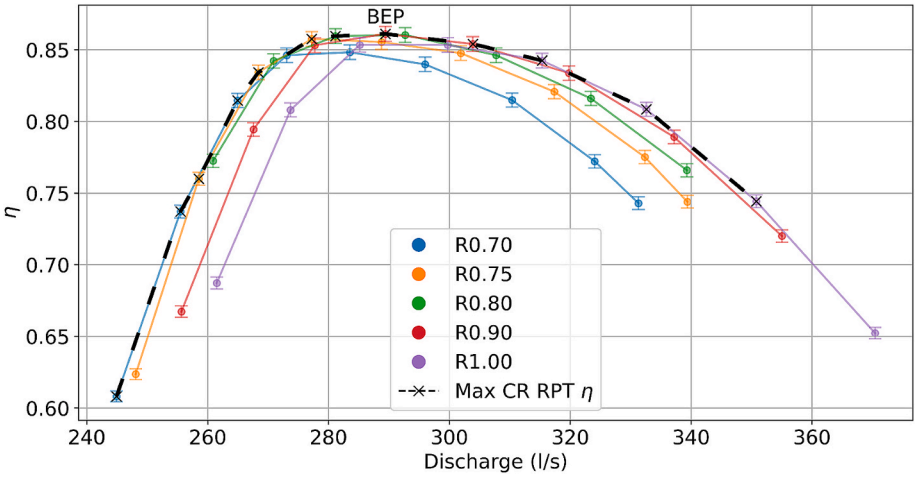

Fig. 8. Efficiency versus discharge of the CR-RPT in turbine mode for all tested speed ratios. Error bands are included for each data point.

Table 4
BEP of the CR-RPT during turbine mode.

η	ω_1(rpm)	ω_2(rpm)	Q(l/s)	T_1(N•m)	T_2 (N•m)	H_T(m)	P_{m1}(kW)	P_{m2}(kW)	P_m(kW)
86.1 %	800	720	289	91.3	98.0	6.16	7.65	7.39	15.0

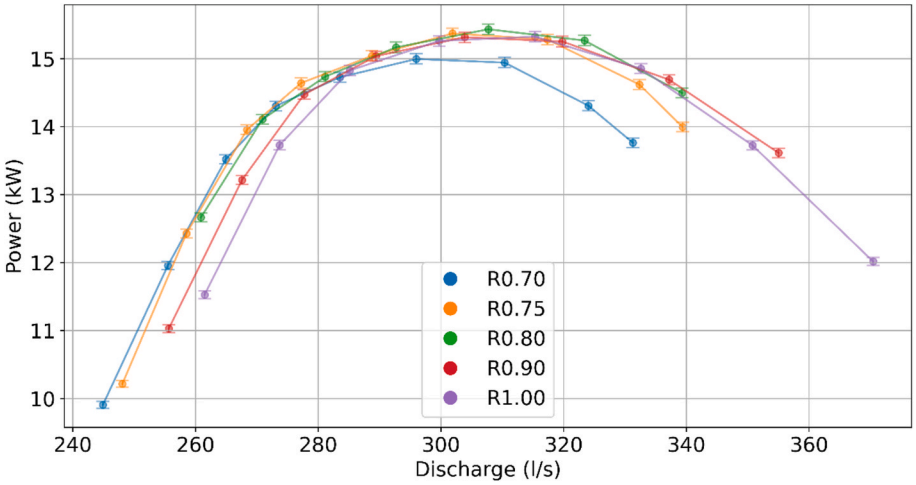

Fig. 9. Mechanical power versus discharge of the CR-RPT in turbine mode for all tested speed ratios. Error bands are included for each data point.

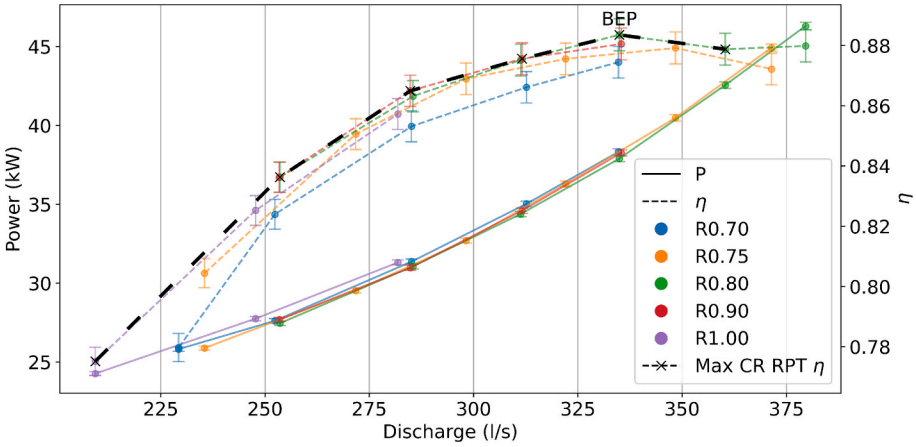

Fig. 10. Power (solid lines) and efficiency (dashed lines) of the CR-RPT in pump mode. Error bands are included for each data point.

Table 5
BEP of CR-RPT during pump mode.

η	ω_1(rpm)	ω_2(rpm)	Q(l/s)	T_1(N•m)	T_2 (N•m)	H_P(m)	P_{m1}(kW)	P_{m2}(kW)	P_m(kW)
88.4 %	1249	1000	335	157	166	10.2	20.5	17.4	37.9

bility. For example, in turbine mode, the produced power can be reduced at 90 % of its maximum value at R0.75 ($Q = 278$ l/s, $H_T = 6.35$ m) in two ways. The first method is to keep the butterfly valve fully opened while reducing the rotational speed to reduce the discharge to 265 l/s, resulting in an efficiency of 95 % of its maximum value. The second method requires setting the butterfly valve to V1/2, achieving 90 % of maximum power at a discharge of 282 l/s and an efficiency of 98 %. Comparing both methods shows that the butterfly valve allows for high discharge and efficiency while reducing power output due to net head reduction. The valve introduces a hydraulic loss in the system, which means that the most efficient points will always be achieved for a V1 scenario. However, if power output reduction is required, the discharge can remain relatively large when the valve is used compared to when it is not. In real operation, the efficiency of the mechanical and electrical components must also be evaluated, as it could influence these results. Nevertheless, the results show that using a valve increases the machine operating conditions compared to solely relying on a fully open valve and adjusting runner speed. These findings align with the study published by Truijen et al. [45].

Dimensionless analysis

To evaluate the full-scale machine characteristics and compare them with other hydraulic machines documented in the literature, dimensionless coefficients are used. Fig. 13 presents dimensionless coefficients for turbine mode, with each speed ratio represented by a different curve.

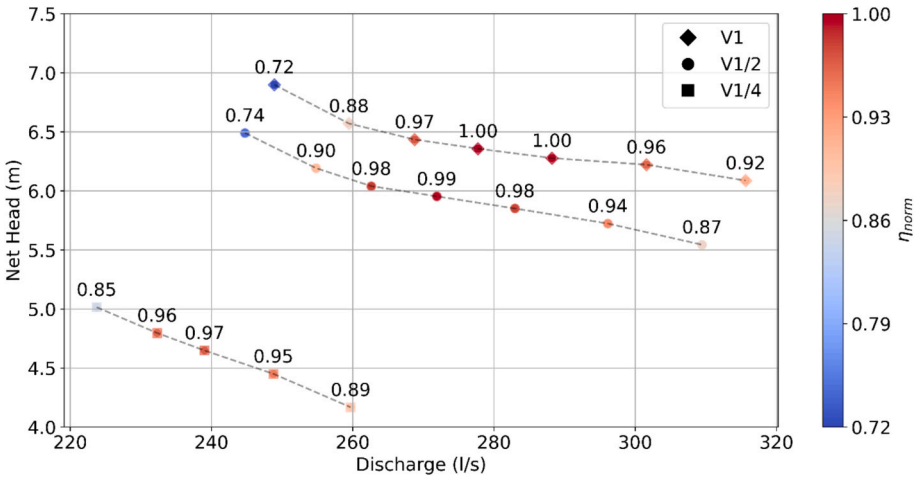

Fig. 11. Net head versus discharge points for turbine mode and R0.75. Data recorded for three different BV1 openings. V1 = fully open valve, normal operation conditions, V1/2 half open valve and V1/4 valve opened at one quarter of its capacity. Colors and numbers show the normalized machine efficiency, corresponding to reduction of maximum efficiency.

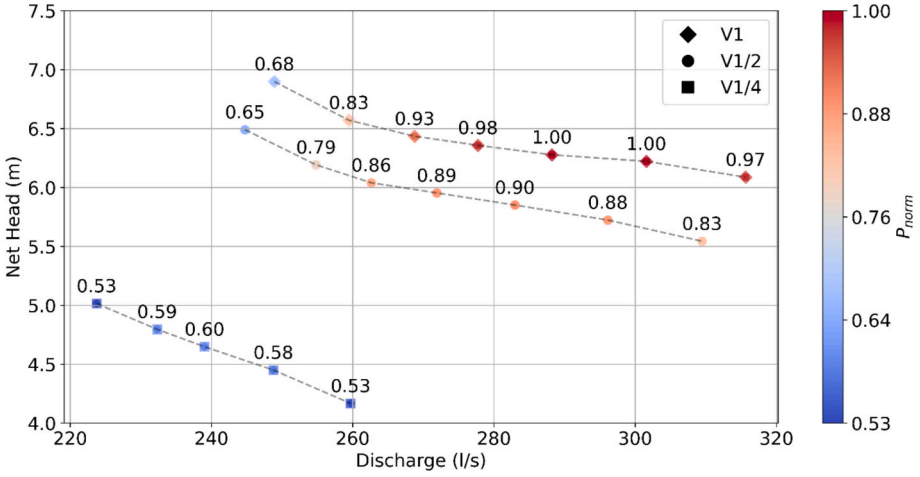

Fig. 12. Net head versus discharge points for turbine mode and R0.75. Data recorded for three different BV1 openings. V1 = fully open valve, normal operation conditions, V1/2 half open valve and V1/4 valve opened at one quarter of its possibilities. Colors and numbers show the normalized power efficiency, corresponding to reduction of maximum power.

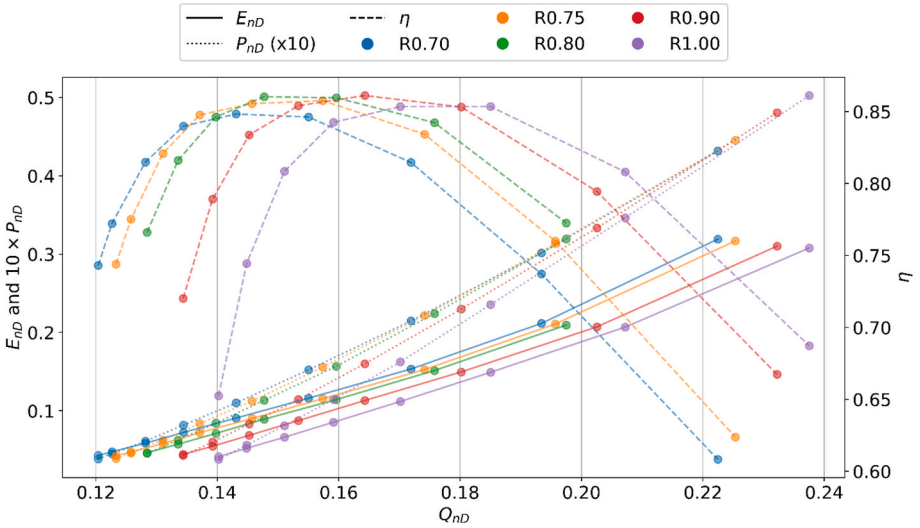

Fig. 13. E_{nD} (solid lines), P_{nD} (dotted lines) and efficiency (dashed lines) characteristic curves of CR-RPT in turbine mode. The P_{nD} is multiplied by a factor of 10 to improve visualization of the plot.

The CR-RPT shows an overall efficiency higher than 80 % for discharge coefficient (Q_{nD}) ranging from 0.125 to 0.21, i.e. from 76 % to 128 % of BEP. The energy coefficient (E_{nD}) ranges from 0.05 (44 % BEP) to 0.27 (238 % BEP). Finally, the power coefficient (P_{nD}) ranges from 0.005 ((29 % BEP) to 0.037 ((218 % BEP). This demonstrates that for a CR-RPT the operation is efficient for a large range of discharge values, in accordance with the results found in Furukawa et al. [18] for a contra-rotating pump.

Fig. 14 presents the dimensionless coefficients for pump mode, showing different characteristics for the different speed ratios. An efficiency above 80 % is kept for Q_{nD} above 0.095 (58 % BEP), E_{nD} above 0.082 (73 % BEP) and P_{nD} above 0.01 (59 % BEP). The upper range of Q_{nD} is not available from the dataset.

The BEP factors in Table 6 allow for upscaling the CR-RPT to the design characteristics of a LH PHS system outlined in the introduction Section, i.e., runner diameter of 6 m and a net head of 9 m. In this conditions, a scaled-up CR-RPT works at BEP with a discharge of 165 m^3/s, producing a power of 12.6 MW, while operating at 86.6 % efficiency. For pump mode at BEP, the power consumption is 14.8 MW, resulting in a discharge of 148 m^3/s, while operating at 88.4 % efficiency. These calculations verify that the CR-RPT operates near the prototype design discharge and power of 130 m^3/s, and 10 MW respectively, as reported by Fahlbeck et al. [20].

The Reynolds number of the prototype affects the scalability of the efficiency as described in Annex F of IEC [31]. According to IEC and Dixon and Hall [14], the efficiency always increases when upscaling. However, Wang et al. [46] recently found that for ultra-low-head (<5 m) scenarios, the efficiency increases according to IEC formulation up to a geometric scale of 16. For larger scale factors, the efficiency drops. Nonetheless, for geometric scales up to $\lambda_L = 32$ the efficiency of both pump and turbine modes remains higher than that of the small-scale model. Thus, the efficiency of a CR-RPT prototype of 6 m in diameter is expected to exceed the efficiency reported in this study. It should be noted that, as the geometric scale in this study is $\lambda_L = 22$, calculating the efficiency with IEC formulation may result in an overestimation. The efficiency reported throughout this study is that found for the model scale CR-RPT, which is the most conservative value.

Comparison of CR-RPT with other hydraulic machines from literature

This Section compares the performance of the CR-RPT to the hydraulic machines presented in Section "Dimensionless parameters for pump-turbine performance".

Turbine mode comparison is summarized in Fig. 15, excluding the high-head machines because Table 2 shows that the BEPs of the three centrifugal PATs ($\Omega_{sp} = 0.22, 0.23, 0.24$) and the Francis turbine from Trivedi et al., [44] ($\Omega_{sp} = 0.42$) are at higher E_{nD} and lower Q_{nD} values compared to the CR-RPT. This is expected as both the PATs and Francis turbines work efficiently under high head conditions. They are included in the comparative analysis for completeness.

In turbine mode (see Fig. 15), the CR-RPT presents one of the largest Q_{nD} and a lowest E_{nD}, reflecting its design considering low-head and high discharge conditions. Only the Bulb turbines from La Rance and Annapolis tidal power plants operate at higher discharge (higher Q_{nD}) and lower head (lower E_{nD}) conditions. A CR-RPT for LH PHS would operate at higher heads (5 m – 30 m [11]), compared to the bulb turbines of both La Rance and Annapolis, which are designed for heads from 3 m to 11 m [36], and 1.4 m to 7.1 m [37], respectively. While both the CR-RPT and the bulb turbine of La Rance operate at a similar maximum efficiency in turbine mode, the CR-RPT works efficiently under a wide range of operating conditions. Unfortunately, data for the bulb turbine of La Rance across these conditions is not available in the literature. Furthermore, La Rance bulb turbine is designed primarily for turbine mode operation, although it can pump water into the reservoir during high tide (at a maximum efficiency of 66 % for 3 m of head, dropping at 48 % for 2 m of head [13]), this is not a main function. The operating range for the Annapolis bulb turbine is also not available and it does not operate in pump mode. An Andritz bulb turbine, as reported in Aggidis and Feather [41], shows both smaller Q_{nD} and E_{nD} compared to the CR-RPT, while maintaining a high specific speed ($\Omega_{sp} = 4.68$). In comparison with the bulb turbines from La Rance and Annapolis, the E_{nD} is similar but the Q_{nD} is halved, indicating that this machine is designed for lower discharge conditions.

The study by Kanemoto et al. [42] (Turbine mode:$\Omega_{sp} = 1.42$, $Q_{nD} = 0.074$, $E_{nD} = 0.110$, $P_{nD} = 7.17 \bullet 10^{-3}$, pump mode: $\Omega_s = 2.13$, $Q_{nD} = 0.055$, $E_{nD} = 0.053$, $P_{nD} = 3.96 \bullet 10^{-3}$) provides performance of a contra-rotating pump turbine, facilitating comparison of a similar type of machine with the CR-RPT. The CR-RPT exhibits larger Q_{nD} and P_{nD} in both pump and turbine modes, indicating that it operates at BEP with larger discharges and power for similar heads and machine sizes. The E_{nD} is similar for both machines, indicating that they operate at similar head values, but the CR-RPT is able to operate with much larger discharges, generating more power. This is advantageous for the CR-RPT as for similar head conditions, and runner diameter, it is able to work with more discharge and power, thus reducing the size of its mechanical components and that of adjacent civil structures when installed in a LH

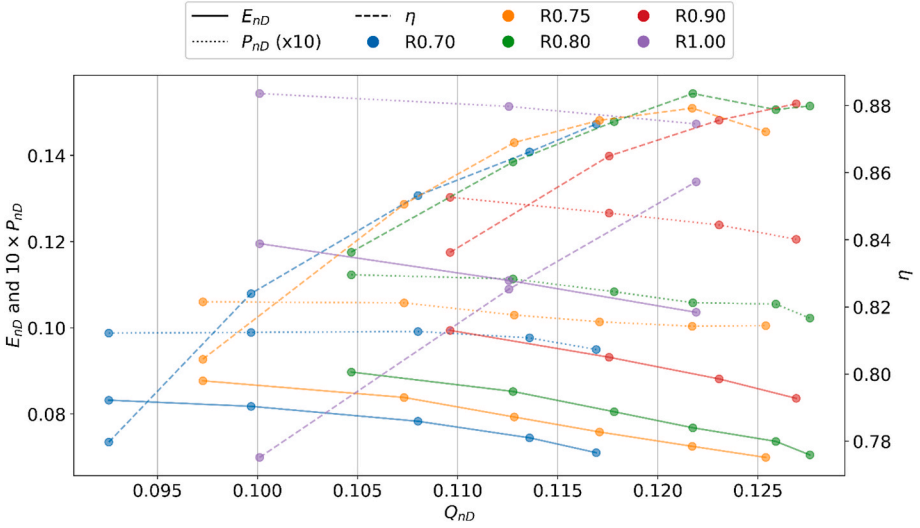

Fig. 14. Dimensionless characteristic curves of CR-RPT in pump mode. E_{nD} (solid lines), P_{nD} (dotted lines) and η (dashed lines) versus Q_{nD} for all tested speed ratios. P_{nD} is multiplied by a factor of 10 to improve visualization of the plot.

Table 6.D
imensionless coefficients and factors at bep for the cr-rpt.

Mode	$\frac{w_2}{w_1}$	η	Q_{nD}	E_{nD}	$T_{1\,nD}$	$T_{2\,nD}$	P_{nD}	Ω_{sp}, Ω_s	Q_{ED}	P_{ED}	n_{ED}
Turbine	0.90	86.1 %	0.164	0.113	0.008	0.009	0.017	1.93	0.489	0.421	2.97
Pump	0.80	88.4 %	0.122	0.077	0.006	0.006	0.012	2.39	0.439	0.497	3.61

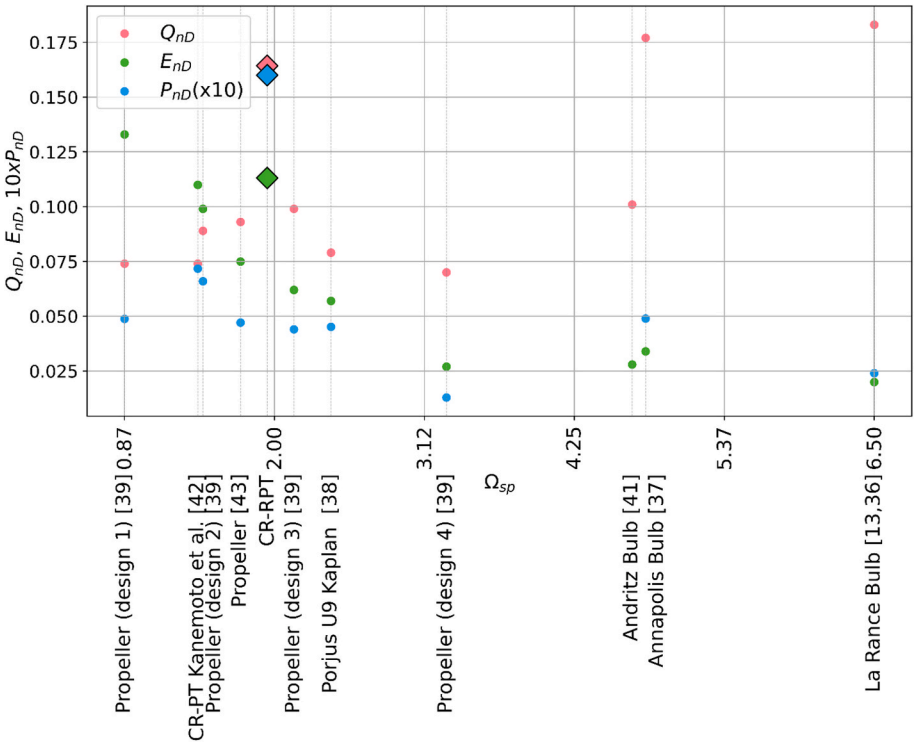

Fig. 15. Comparison of dimensionless coefficients between the CR-RPT (diamond shaped points) in turbine mode and the turbines included in Table 2 (circular shaped points). The high-head machines from Table 2 are not represented. $\boldsymbol{Q_{nD}}$ is shown in red color, $\boldsymbol{E_{nD}}$ in green color, and $\boldsymbol{P_{nD}}$ in blue color. $\boldsymbol{P_{nD}}$ is multiplied by a factor of 10 to improve visualization of the plot. (For interpretation of the references to color in this figure legend, the reader is referred to the web version of this article.)

PHS system.

Alexander et al. [39] disclosed the turbine performance of four different propeller type axial-flow turbines for microhydro systems (propeller 1 $\Omega_{sp} = 0.87$, propeller 2 $\Omega_{sp} = 1.5$, propeller 3 $\Omega_{sp} = 2.1$, propeller 4 $\Omega_{sp} = 3.3$). Propeller 1 works at slightly larger E_{nD} and much lower Q_{nD}. Propeller 2, 3 and 4 work at lower E_{nD} and Q_{nD} compared to the CR-RPT. While the Ω_{sp} of propeller 3 is comparable to that of the CR-RPT, the CR-RPT has higher coefficients overall, therefore operating at higher discharge, heads, and power levels while keeping more compact dimensions and lower rotational speeds. However, the performance at off-design points for these propeller turbines is not reported. It is also noted that higher the Ω_{sp} values correlate with lower efficiencies, suggesting room for improvement for the propeller designs with similar Ω_{sp} to that of the CR-RPT. It should be noted that the propeller turbines reported in Alexander et al. [39] utilize planar runners for simple manufacturing. Although the authors report potential for efficiency improvements, they are not quantified. The reported efficiencies ranging from 68 % to 74 % are far from that of the CR-RPT. The performance of these propeller type turbines was not evaluated in pump mode.

The propeller turbine from Samora et al., [43] and the Porjus U9 Kaplan are close to the CR-RPT in terms of Ω_{sp} but they present lower values for Q_{nD}, E_{nD} and P_{nD} overall. This shows again that the CR-RPT can work with larger heads, discharges and power when compared to machines with similar Ω_{sp}.

According to Dixon and Hall [32] the theoretical Ω_{sp} ranges for different types of machines are from 0.2 to 2.0 for Francis turbines, 2.0 to 3.5 for propeller turbines, and 2.5 to 6.0 for Kaplan turbines. This aligns with the findings of this study as the three different PATs have a Ω_{sp} of 0.22, 0.23, and 0.24. The propeller turbines from Alexander et al. [39] have values of 0.9, 1.5, 2.1 and 3.3, ranging around the values for propeller turbines and going to the limits of Francis and Kaplan turbines. The contra-rotating machine from Kanemoto et al. [42] has a Ω_{sp} value of 1.42, very similar to that of the CR-RPT. Additionally, the propeller machine from Samora et al., and the Porjust U9 Kaplan present a Ω_{sp} of 1.74 and 2.42 respectively. These two machines present values slightly lower than those reported in Dixon and Hall [32]. The CR-RPT has a Ω_{sp} value of 1.9, coinciding with propeller turbines. The bulb turbines for La Rance, Annapolis and Andritz have a Ω_{sp} of 6.5, 4.8, and 4.68, residing in the high-end range of Kaplan turbines.

Due to the limited data available in the literature on low-head pump performance, comparisons in pump mode are inconclusive. However, data for a low-head pump reported by Jiao et al. [40], shows that it indeed works at high discharge low head conditions, with an Ω_s of 5.95. Its dimensionless coefficients ($Q_{nD} = 0.064$, $E_{nD} = 0.020$, $P_{nD} = 0.002$) are less than half of those of the CR-RPT suggesting that the CR-RPT works with significantly larger discharge, head and power. The pump from Jiao et al. [40] has characteristics that better resembles the bulb turbine of La Rance working in pump mode, therefore it is likely not efficient for LH PHS. Furthermore, the efficiency is significantly lower (67 %) than that of the CR-RPT, and its off-design performance data is not available.

To conclude the comparison, Fig. 16 illustrates the operating conditions under which the reported machines would operate efficiently at a head of 9 m and a runner diameter of 6 m. The CR-RPT works as reported in Section "Results from the CR-RPT test rig", while the counter-rotating pump-turbine from Kanemoto et al. [42] would require a lower discharge to keep efficiency high, penalizing power output. Both machines have similar rotational speeds. In contrast, the bulb turbines would need significantly larger discharge and rotational speeds compared to the CR-RPT to operate efficiently under the desired conditions. Using two CR-RPT units working at lower discharge and rotational speeds would be more advantageous, as this configuration produces a similar power output while reducing the discharge rate. This is beneficial for storage capacity, as a larger discharge at a fixed volume results in shorter operating storage time scale for the LH PHS. Additionally, bulb turbines do not operate or operate inefficiently in pump mode. These aspects present significant advantages for the CR-RPT in a LH PHS system. Propeller 4 exhibits similar discharge values to the CR-RPT, but propeller 4 produces less power while operating at larger rotational speed and its efficiency is significantly lower than that of the CR-RPT. Thus, it is found that the CR-RPT operates more efficiently for the conditions required in a LH PHS system compared to the machines reported in literature.

Limitations of the present study

Several practical insights were gained during execution of the CR-RPT tests, which provide valuable information for improving the experimental methodology and understanding the operational intricacies of the CR-RPT.

The use of two open surface water tanks for adjusting the gross head of the test is unique in the literature concerning pump, turbine or pump-turbine characterization tests. This is expected to give more realistic conditions than when using a closed-loop system, particularly when studying transients. However, one of the issues identified in the LWI CR-RPT test rig is the occurrence of swirl, it may occur because the lower tank is fed via pipe 2, which is perpendicular to the spillway. When the water jet from pipe 2 hits the spillway, it is diverted left and right, creating two circular currents in the lower tank that may affect the water entering pipe 1 (see Fig. B.1). This could create a swirl flow, negatively impacting the CR-RPT performance in pump mode, yet its actual existence and effects were not quantified, representing a limitation that could impact pump performance and cavitation. This study calculates net head by static pressure difference before and after the runners, which is only true if there is no swirl as the fluid axial velocities are the same before and after the runners (assuming no boundary layers).

A notable limitation of this study is the inability to collect performance data at different gross heads. Future studies should assess the performance of the CR-RPT for variable gross head inputs, particularly if the machine is intended for installation in a LH PHS system.

Given that the CR-RPT may operate in a LH PHS system in a marine environment, several factors should be considered. The larger density of seawater will likely increase the hydraulic power (see Eq. (6)), while its larger viscosity may result in a larger friction loss, likely reducing both the net head and discharge thus reducing hydraulic power. At the same time, denser seawater may also increase the runners' torque and thus mechanical power. Although these effects were not quantified in this study, they could be minor given that seawater is approximately 3 %

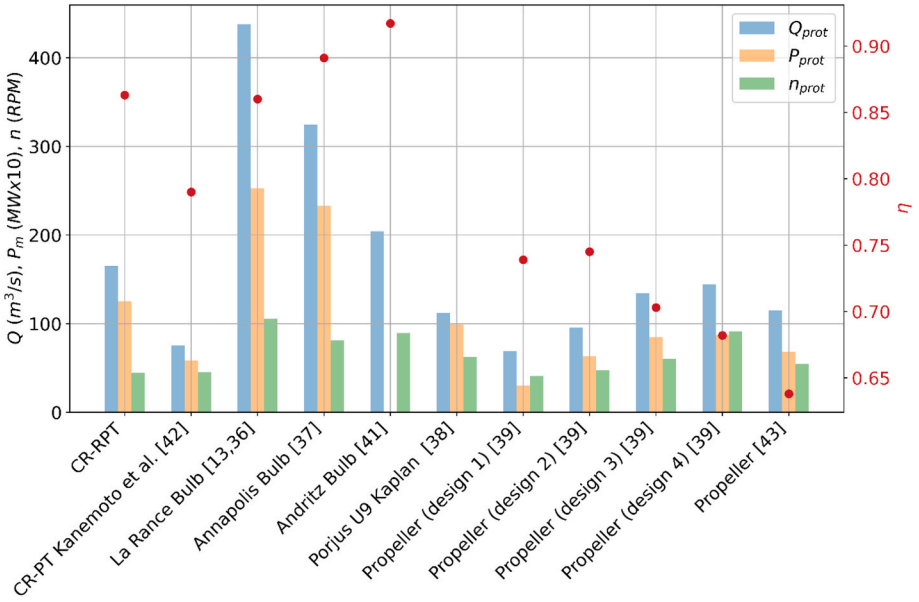

Fig. 16. Comparison of characteristics of turbines for a head of 9 m and a diameter of 6 m. The power has been multiplied by a factor of 10 to improve plotting visualization. The red dots represent the efficiency as reported in Table 2. (For interpretation of the references to color in this figure legend, the reader is referred to the web version of this article.)

denser and 8 % more viscous. Nonetheless, they should be taken into account when considering the CR-RPT for an LH PHS system. Furthermore, long-term effects of salty water and biofouling to both materials and performance should be studied.

Lastly, the runners used during the laboratory tests represent an early design. Consecutive iterations will likely improve the efficiency and working range of the runners.

Conclusion

This study evaluated the performance of a CR-RPT using a custom-built test rig in the LWI laboratory and compared it to that of other hydraulic machines documented in the literature.

The CR-RPT achieves over 80 % efficiency across a wide range of operating conditions. Notably, in turbine mode, an efficiency above 80 % is maintained for discharge coefficients ranging from 76 % to 128 % of BEP, head coefficients from 44 % to 238 %, and power coefficients from 29 % to 218 %. In pump mode the 80 % efficiency threshold begins at 58 %, 73 % and 59 % for the discharge, head and power coefficients, respectively. The upper efficiency boundary was not reached during the tests presented in this study due to cavitation.

Moreover, the use of a butterfly valve further increased the operating range of the machine in turbine mode. When, by the use of the butterfly valve, the net head is reduced to 72 % of its maximum value (i.e. for a fully opened butterfly valve), and the discharge decreased to 86 % of its original value, the efficiency remained at 97 % of the maximum. Such operating point could not be achieved without the use of the butterfly valve, thus increasing the efficient operating range of the CR-RPT.

The CR-RPT tested for this study shows unique specific speeds when compared to other hydraulic machines ($\Omega_{sp} = 1.93$ in turbine mode and a $\Omega_s = 2.39$ in pump mode). Furthermore, it exhibits the highest power coefficient at BEP among the machines reviewed, both in turbine ($P_{nD} = 0.017$, 7 times larger than that of the bulb turbine of La Rance and 3 times larger than that of the Annapolis bulb turbine) and pump modes ($P_{nD} = 0.012$). This advantage enables the machine to operate at a larger power for the same rotational speed and size. As a result, large amounts of energy can be stored and produced using a relatively compact machine. This compactness reduces the mechanical and civil engineering works necessary for constructing a CR-RPT prototype, as fewer pump-turbine units are needed to achieve large power inputs and outputs.

The findings of this study confirm the viability of the CR-RPT as a unique, high performance option for LH PHS systems.

Future work is recommended to investigate the performance of the machine at multiple gross head conditions and to test for cavitation inception. Furthermore, the analysis of flow patterns and their influence on performance may provide valuable insights to optimize CR RPT runner geometry for LH PHS systems.

Funding sources

This study was supported by the European Union Horizon 2020 project ALPHEUS (Augmenting grid stability through Low-head Pumped Hydro Energy Utilization & Storage) project ID 88355.

CRediT authorship contribution statement

Ruben Ansorena Ruiz: Writing – review & editing, Writing – original draft, Visualization, Validation, Software, Resources, Methodology, Investigation, Formal analysis, Data curation, Conceptualization. **David Schürenkamp:** Writing – review & editing, Supervision, Project administration. **Daan P.K. Truijen:** Writing – review & editing, Resources, Investigation, Conceptualization. **Justus P. Hoffstaedt:** Writing – review & editing, Resources, Investigation, Conceptualization. **Antonio Jarquin Laguna:** Writing – review & editing, Supervision, Resources, Project administration, Methodology, Investigation, Funding acquisition, Conceptualization. **Jonathan Fahlbeck:** Writing – review & editing, Resources, Conceptualization. **Håkan Nilsson:** Writing – review & editing, Supervision, Project administration, Funding acquisition, Conceptualization. **Melvin Joseph:** Writing – review & editing. **Mehrdad Zangeneh:** Writing – review & editing. **Jeroen D.M. De Kooning:** Writing – review & editing, Supervision, Project administration, Funding acquisition. **Jonas Oldeweme:** Writing – review & editing. **Heiko Schwarz:** Writing – review & editing. **Nils Goseberg:** Writing – review & editing, Writing – original draft, Supervision, Project administration, Methodology, Funding acquisition, Conceptualization.

Declaration of competing interest

The authors declare the following financial interests/personal relationships which may be considered as potential competing interests: Ruben Ansorena Ruiz reports financial support was provided by Horizon 2020 European Innovation Council Fast Track to Innovation. If there are other authors, they declare that they have no known competing financial interests or personal relationships that could have appeared to influence the work reported in this paper.

Acknowledgments

This paper was funded by the European Union Horizon 2020 project ALPHEUS (Augmenting grid stability through Low-head Pumped Hydro Energy Utilization & Storage) project ID 883553.

Appendix A:. Mechanical design of the CR-RPT

The mechanical drawing in this appendix particularly shows the design of the internal shafts and bevel gears. The motor shafts are positioned inside two of the support struts. The transparent pipe made of acrylic glass, surrounding the runners, is not included in the drawing. The drawing is not to scale.

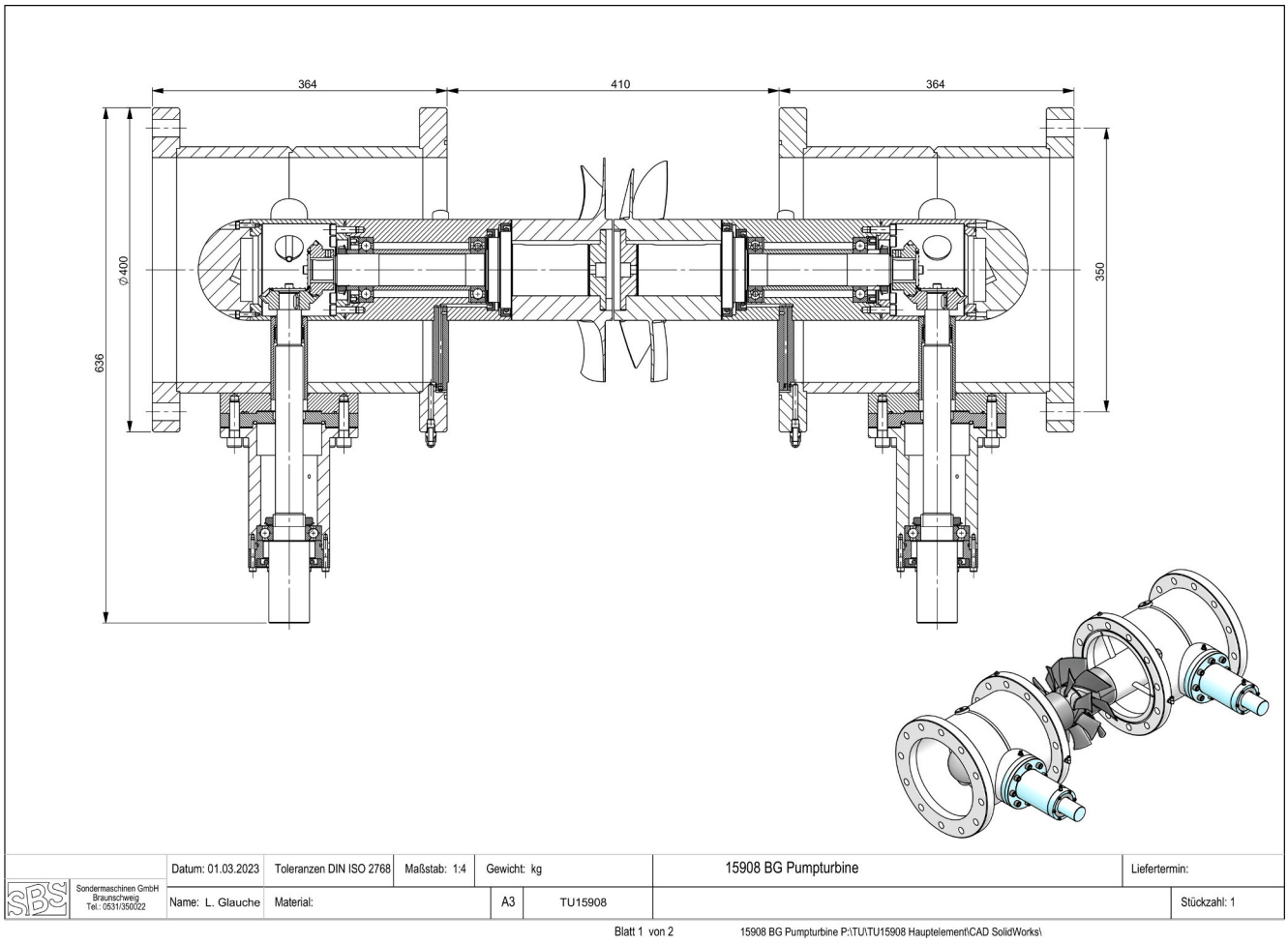

Mechanical drawing of CR-RPT.

Appendix B:. Test rig error calculation

Precision of the data acquisition equipment

The operations performed for evaluating CR-RPT performance are additions, subtractions, multiplications and divisions. Thus, error formulation is given for these. For addition and subtraction:

$$\Delta Z = \sqrt{\sum_{n=1}^{n} (\Delta x_i)^2} \tag{B.1}$$

where ΔZ is the absolute uncertainty in a measurement, Δx_i is the absolute uncertainty in the quantities x_i, and n are the number of measurements. For multiplication and division operations the error is propagated as:

$$\Delta Z = Z \times \sqrt{\sum_{n=1}^{n} \left(\frac{\Delta x_i}{x_i}\right)^2} \tag{B.2}$$

where Z is the result of the multiplication or division, and x_i are the quantities being multiplied or divided.

The maximum relative errors for each measured parameter are summarized in Table 1. Using these relative errors and the error propagation formulas from Eq. (B.1) and Eq. (B.2), the relative errors of the post-processed parameters are calculated and shown in Table 3.

Data differences between accelerated and decelerated setpoints

A comparison of accelerated versus decelerated data in turbine mode shows very little differences. The 95th percentile of the absolute relative errors for 34 data points is less than 0.84 %. The maximum error is for T1 at 2.01 %, considered an outlier typical in real test rig scenarios. Table B1 includes the absolute relative error differences for all the studies parameters at the test rig.

Table B1
Relative errors between accelerating versus decelerating setpoints in turbine and pump mode. "Q2" is the median, "Q3" is the 75th percentile, "P95" is the 95th percentile and "MAX" is the maximum error. Numbers are expressed as a percentage (%).

Mode	Turbine				Pump			
Calculation	Median	Q3	P95	MAX	Median	Q3	P95	MAX
ω1	0.00	0.00	0.01	0.01	0.03	0.04	0.06	0.07
ω2	0.00	0.00	0.01	0.01	0.01	0.02	0.03	0.03
p1	0.04	0.06	0.13	0.24	2.98	6.56	9.48	12.44
p2	0.03	0.06	0.13	0.14	2.73	4.87	7.44	8.60
p3	0.14	0.23	0.28	0.51	5.11	8.80	27.59	42.11
p4	0.13	0.22	0.37	0.59	2.11	5.92	9.25	11.29
p5	0.13	0.30	0.57	0.63	4.83	15.31	564.70	1231.22
p6	0.21	0.41	0.75	1.17	5.50	17.24	494.19	1023.57
p7	0.08	0.11	0.18	0.23	0.17	0.24	0.40	0.45
p8	0.14	0.19	0.36	0.43	0.17	0.27	0.41	0.47
p9	0.03	0.05	0.09	0.11	0.03	0.25	0.29	0.29
p10	0.03	0.04	0.06	0.12	0.09	0.15	0.24	0.27
p11	0.03	0.07	0.33	0.42	0.03	0.04	0.07	0.08
p12	0.02	0.03	0.06	0.07	0.02	0.05	0.06	0.07
Q	0.10	0.13	0.22	0.26	0.39	0.88	1.61	1.86
T_1	0.39	0.59	0.89	2.35	1.52	3.14	4.10	5.02
T_2	0.33	0.48	0.84	1.01	1.45	2.18	3.19	3.53
T_h	0.14	0.19	0.29	0.32	0.29	0.81	1.16	1.30
P_h	0.14	0.26	0.35	0.37	0.19	0.56	1.06	1.07
P_{m1}	0.40	0.59	0.89	2.36	1.47	3.10	4.08	5.00
P_{m2}	0.33	0.48	0.84	1.01	1.48	2.17	3.19	3.51
P_m	0.11	0.27	0.41	0.50	0.63	1.16	1.67	1.86
η	0.19	0.32	0.56	0.75	0.89	1.16	1.93	2.27

For pump mode however, larger differences are observed (see Table B1). An analysis of 13 data points revealed large relative errors for the low-pressure side static pressure sensors, especially for pressure sensors p5 and p6 which are next to the runners. This is due to the values of pressure in these probes being close to zero. The torque measurements showed large errors in pump mode due to the maximum discharge capacity of the pipe 2 of 330 l/s, as pump setpoints operating at larger discharges causes the water level in the lower tank to slowly decreases. Typically, the tests begin at lower speeds and then accelerate to higher speeds before decelerating back to lower speeds. Consequently, the higher speed setpoints have a slightly reduced water level in the lower tank. The maximum water level drop is lower than 10 cm. However, this is around a 5 % of the total height of water above the centerline of pipe 1 and therefore it may be significant for some setpoints. Additionally, it is slightly worst for cavitation, increasing the probability of it appearing.

For lower speed decelerated setpoints, the water level in the lower tank returned to its maximum level, resulting in similar data for decelerated and accelerated setpoints. Table B1 shows that for the low-pressure sensor measurements, half of the relative errors between accelerated and decelerated points are within the rage of 2.1 % to 5.5 %, coinciding with low-speed setpoint data.

Sensitivity analysis of time averaging

Table B2 presents the absolute relative differences for turbine mode parameters calculated using various averaging times (30 s and 20 s) compared to the standard 40 s. The maximum relative error is 1.06 %, with negligible variations for 30 s and 20 s averaging times. While p6 and T1 exhibited larger maximum errors, the 95th percentile remained stable across pressure probes, confirming that varying the averaging time had minimal influence on turbine mode results. The larger averaging time of 40 s was chosen for calculating machine performance values as it ensures a more complete representation of the steady state.

Table B2
Absolute difference between parameters calculated using different averaging times, compared to the normal 40 s averaging time for turbine mode. "Q2" is the median, "Q3" is the 75th percentile, "P95" is the 95th percentile and "MAX" is the maximum error. Numbers are expressed as a percentage (%).

Mode	Turbine							
Averaging time	30				20			
Calculation	Q2	Q3	P95	MAX	Q2	Q3	P95	MAX
ω1	0.00	0.00	0.01	0.01	0.00	0.01	0.01	0.01
ω2	0.00	0.00	0.01	0.01	0.00	0.01	0.01	0.01
p1	0.01	0.02	0.06	0.12	0.02	0.04	0.11	0.17
p2	0.01	0.02	0.04	0.07	0.02	0.04	0.10	0.18
p3	0.06	0.11	0.22	0.39	0.08	0.19	0.39	0.52
p4	0.03	0.08	0.17	0.43	0.09	0.17	0.39	0.65
p5	0.06	0.13	0.27	0.57	0.12	0.21	0.57	0.85
p6	0.07	0.14	0.34	1.03	0.15	0.27	0.65	1.06
p7	0.01	0.02	0.04	0.06	0.02	0.04	0.07	0.11
p8	0.02	0.03	0.05	0.08	0.04	0.07	0.11	0.18
p9	0.01	0.01	0.02	0.09	0.01	0.02	0.04	0.10
p10	0.00	0.01	0.02	0.03	0.01	0.02	0.03	0.08
p11	0.00	0.01	0.01	0.51	0.01	0.01	0.03	0.51
p12	0.00	0.01	0.01	0.02	0.01	0.01	0.02	0.06

(*continued on next page*)

Table B2 (*continued*)

Mode	Turbine							
Averaging time	30				20			
Calculation	Q2	Q3	P95	MAX	Q2	Q3	P95	MAX
Q	0.03	0.05	0.08	0.23	0.04	0.09	0.13	0.27
T_1	0.06	0.11	0.39	0.81	0.14	0.24	0.65	1.02
T_2	0.06	0.10	0.20	0.54	0.11	0.22	0.43	0.51
T_h	0.27	0.34	0.46	0.50	0.27	0.37	0.44	0.63
P_h	0.28	0.35	0.45	0.56	0.29	0.36	0.51	0.59
P_{m1}	0.06	0.11	0.40	0.81	0.14	0.24	0.66	1.03
P_{m2}	0.06	0.11	0.20	0.53	0.11	0.22	0.43	0.51
P_m	0.02	0.03	0.06	0.68	0.04	0.06	0.14	0.66
η	0.29	0.36	0.45	0.62	0.29	0.34	0.46	0.54

For pump mode 23 points are analyzed and, compared to turbine mode, larger relative errors are observed, particularly at the low-pressure side probes. Turbulent flow conditions in the lower tank during pump mode contributed to this discrepancy. This can be explained from the water motion within the lower tank during pump mode, which shows two circular patterns. Looking at it from a top view perspective, see Fig. B1, the water enters the lower tank via pipe 2, causing a water jet perpendicular to the spillway which is diverted towards the left and right. Each diversion creates a circular water flow path within the lower tank. It should be noted that in the connection between pipe 1 and the lower tank, exists an oblique water flow, respecting the direction of the water within pipe 1, from left to right in Fig. B1. This can cause a swirl within pipe 1 that could, in turn, affect the measurements in the pressure probes as a dynamic pressure component may be present together with the static pressure component. In contrast, during turbine mode the long pipe 1 length before reaching the CR-RPT, reduces the swirl in the water before the CR-RPT. After the CR-RPT, Runner 2 will compensate for the swirl created by Runner 1 and therefore at the low-pressure side, low swirl is expected.

Table B3 shows the statistical distribution of the absolute relative errors showing that 95th percentile is affected by the errors at maximum speed. For the data points that are not at maximum speed (17 points), the maximum error is kept below 1 %.

Table B3
Relative difference between parameters calculated using different averaging times, compared to the normal 40 s averaging time for turbine mode. "Q2" is the median, "Q3" is the 75th percentile, "P95" is the 95th percentile and "MAX" is the maximum error. Numbers are expressed as a percentage (%).

Mode	Pump							
Averaging time	20				15			
Calculation	Median	Q3	P95	MAX	Median	Q3	P95	MAX
ω1	0.02	0.04	0.05	0.06	0.02	0.05	0.08	0.09
ω2	0.01	0.02	0.02	0.03	0.01	0.02	0.04	0.04
p1	0.27	0.39	0.74	0.89	0.39	0.59	1.17	1.39
p2	0.05	0.09	0.26	0.30	0.12	0.18	0.26	0.31
p3	0.40	0.78	2.24	3.77	0.54	1.00	2.37	7.32
p4	0.13	0.32	0.52	0.58	0.18	0.46	0.73	1.51
p5	0.71	1.36	46.23	114.24	1.18	1.71	177.99	286.19
p6	0.59	1.85	140.81	449.19	1.00	2.56	25.59	1134.95
p7	0.05	0.07	0.13	0.32	0.05	0.08	0.12	0.26
p8	0.02	0.04	0.13	0.17	0.03	0.07	0.13	0.17
p9	0.02	0.03	0.07	0.15	0.02	0.04	0.12	0.14
p10	0.02	0.03	0.05	0.12	0.02	0.04	0.07	0.10
p11	0.01	0.01	0.03	0.05	0.01	0.02	0.04	0.04
p12	0.01	0.01	0.03	0.03	0.01	0.02	0.03	0.04
Q	0.06	0.10	0.14	0.15	0.11	0.18	0.25	0.45
T_1	0.36	0.67	1.45	2.71	0.47	1.01	1.72	1.98
T_2	0.22	0.39	0.71	1.81	0.29	0.62	1.06	1.15
T_h	0.18	0.22	0.27	0.37	0.19	0.25	0.30	0.37
P_h	0.16	0.22	0.33	0.37	0.19	0.29	0.43	0.51
P_{m1}	0.37	0.69	1.41	2.67	0.48	0.97	1.65	1.98
P_{m2}	0.21	0.38	0.69	1.80	0.27	0.59	1.07	1.14
P_m	0.08	0.18	0.35	0.69	0.12	0.25	0.41	0.78
η	0.18	0.27	0.47	0.91	0.15	0.25	0.55	0.70

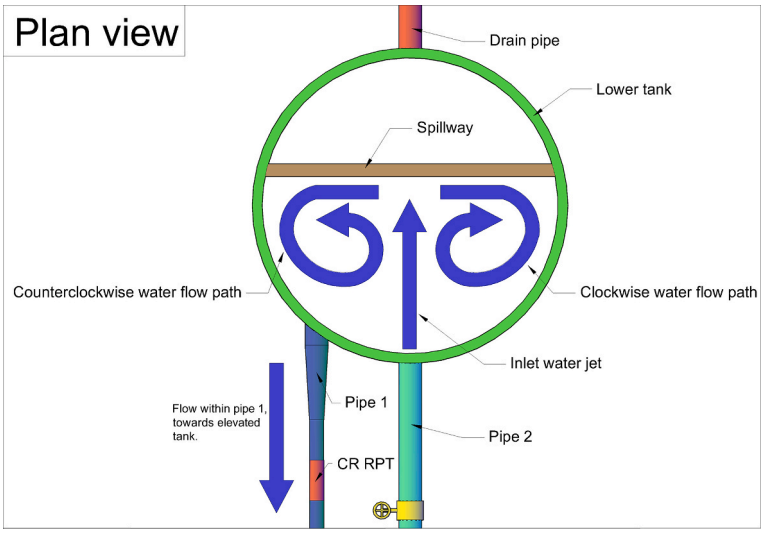

Fig. B.1. Plan view sketch of the water paths within the lower tank (green) during pump mode operation.

Repeatability of the tests

To evaluate the consistency of the recorded data, certain setpoints were tested on different days. For example, the setpoint $n_1 = 800$ rpm, $n_2 = 800$ rpm was performed on two different testing days. Data from both tests is then post-processed and compared, although theoretically identical, variations arise from the stochastic nature of laboratory testing.

In turbine mode 33 distinct setpoints were repeated, with some setpoints repeated more than once resulting in 52 different comparisons. The results are summarized in Table B4.

Table B4
Absolute relative difference between setpoints tested on different testing days in turbine mode. "Q2" is the median, "Q3" is the 75th percentile, "P95" is the 95th percentile and "MAX" is the maximum error. Numbers are expressed as a percentage (%).

Mode	Turbine				Pump			
Calculation	Median	Q3	P95	MAX	Median	Q3	P95	MAX
ω1	0.01	0.04	0.04	0.04	0.04	0.05	0.11	0.13
ω2	0.00	0.03	0.03	0.03	0.03	0.99	7.07	11.11
p1	0.15	2.32	2.32	2.32	2.32	4.97	10.31	11.93
p2	0.14	1.49	1.49	1.49	1.49	3.24	8.38	9.64
p3	0.35	4.07	4.07	4.07	4.07	8.96	44.25	66.71
p4	0.33	3.24	3.24	3.24	3.24	5.94	17.26	24.75
p5	0.53	29.09	29.09	29.09	29.09	90.30	561.11	563.60
p6	0.61	43.72	43.72	43.72	43.72	108.38	743.10	897.39
p7	0.43	0.12	0.12	0.12	0.12	0.40	0.70	0.83
p8	0.34	0.44	0.44	0.44	0.44	0.61	1.05	1.15
p9	0.12	0.16	0.16	0.16	0.16	0.19	0.92	1.32
p10	0.12	0.13	0.13	0.13	0.13	0.32	0.56	0.72
p11	1.97	0.25	0.25	0.25	0.25	0.38	1.14	1.14
p12	0.07	0.13	0.13	0.13	0.13	0.22	0.47	0.62
Q	0.19	0.67	0.67	0.67	0.67	1.13	4.47	6.05
T_1	1.31	3.10	3.10	3.10	3.10	5.01	7.86	9.36
T_2	0.99	1.68	1.68	1.68	1.68	2.66	11.66	15.68
T_h	0.53	0.38	0.38	0.38	0.38	0.64	2.27	3.35
P_h	0.69	0.91	0.91	0.91	0.91	1.45	6.08	9.14
P_{m1}	1.31	3.09	3.09	3.09	3.09	4.96	7.83	9.31
P_{m2}	1.03	2.59	2.59	2.59	2.59	2.72	17.53	25.47
P_m	1.12	0.97	0.97	0.97	0.97	1.23	5.67	8.35
η	1.00	0.34	0.34	0.34	0.34	0.48	0.89	0.93

Turbine mode data in Table B.4 indicate that higher differences are mainly associated to the low-pressure side pressure sensors, followed by errors in torque measurements at the 95th percentile and maximum values. Most of the points in turbine mode demonstrate very low relative errors, with around half of the points showing errors lower than 1 %. This indicates that the test rig in turbine mode produced consistent values regardless of the day on which the tests were conducted.

For pump mode 5 points were repeated more than once, 4 of them on two different days for a total of 9 setpoint comparisons. The reduced number is due to the fact that pump mode was more demanding for the test rig. It is also true that pump mode includes less operation points when compared to turbine mode.

The pump mode repeatability setpoints present a larger error when compared to the turbine mode case. We see that 6 out of 9 points are mostly

with relative error lower than 1 %. However, for parameters such as the low-pressure side static pressure and torques, this error is larger. The repeated setpoints were the following:

- $\omega1 = \omega2 = 1000$ rpm
- $\omega1 = 1100$ rpm ($\omega2/\omega1 = 0.9$), repeated on two different days
- $\omega1 = 1200$ rpm ($\omega2/\omega1 = 0.7$), repeated on two different days
- $\omega1 = 1200$ rpm ($\omega2/\omega1 = 0.8$), repeated on two different days
- $\omega1 = 1200$ rpm ($\omega2/\omega1 = 0.9$), repeated on two different days

The repeated setpoints occur at high speed where the cavitation risk is higher. It is thus possible that cavitation and large flow separation affected the high speed setpoints, making it challenging to reproduce similar values consistently. In fact, the $n_1 = n_2 = 1000$ rpm setpoint includes a maximum relative error of 6 % and 3 % for p5 and p6 respectively. The rest of the parameters such as torque, pump head, power and efficiency all have errors of 0.18 %, 0.48 %, 0.21 %, 0.44 % and 0.13 % respectively. Suggesting that at low speeds, repeating setpoints does not significantly alter the recorded data. Nevertheless, the analysis would benefit from repeating more low speeds points. Remarkably the maximum relative error for efficiency is just 0.93 %, suggesting that errors in both hydraulic and mechanical torque are balanced even in the presence of cavitation.

Data availability

The data used in this article is available at: https://doi.org/10.24355/dbbs.084-202412181712-0.

References

[1] Pumped storage hydropower: Water batteries for solar and wind powerPumped storage hydropower n.d. https://www.hydropower.org/factsheets/pumped-storage (accessed August 29, 2024).
[2] Blakers A, Stocks M, Lu B, Cheng C. A review of pumped hydro energy storage. Prog Energy 2021;3:022003. https://doi.org/10.1088/2516-1083/abeb5b.
[3] Rehman S, Al-Hadhrami LM, Alam MM. Pumped hydro energy storage system: a technological review. Renew Sustain Energy Rev 2015;44:586–98. https://doi.org/10.1016/j.rser.2014.12.040.
[4] Rijkswaterstaat (RWS), Hollandsche Beton Groep NV, Ballast Nedam Groep NV, Raadg. Ing. Bur. Lievense. Pomp accumulatie centrale Brouwersdam en IJsselmeer (Hoofdrapportage fase 2). Rijkswaterstaat; 1986.
[5] de Boer WW, Verheij FJ, Zwemmer D, Das R. The Energy Island – An Inverse Pump Accumulation Station 2007.
[6] De Boer W, Verheij F, Moldovan N, Van der Veen W, Groe-man F, Schrijner M, et al. Energie-eiland, de haalbaarheid van drie verschillende opties van energieopslag voor Nederland 2007.
[7] Delta21. Delta21 n.d. https://www.delta21.nl/ (accessed August 29, 2024).
[8] Lavooij H, Berke L. UPDATE 2019: DELTA21 2019.
[9] ALPHEUS: Augmenting Grid Stability Through Low Head Pumped Hydro Energy Utilization and Storage. ALPHEUS H2020 n.d. https://alpheus-h2020.eu/ (accessed August 29, 2024).
[10] Prasasti EB, Aouad M, Joseph M, Zangeneh M, Terheiden K. Optimization of pumped hydro energy storage design and operation for offshore low-head application and grid stabilization. Renew Sustain Energy Rev 2024;191:114122. https://doi.org/10.1016/j.rser.2023.114122.
[11] Ansorena Ruiz R, de Vilder LH, Prasasti EB, Aouad M, De Luca A, Geisseler B, et al. Low-head pumped hydro storage: a review on civil structure designs, legal and environmental aspects to make its realization feasible in seawater. Renew Sustain Energy Rev 2022;160:112281. https://doi.org/10.1016/j.rser.2022.112281.
[12] Hoffstaedt JP, Truijen DPK, Fahlbeck J, Gans LHA, Qudaih M, Laguna AJ, et al. Low-head pumped hydro storage: a review of applicable technologies for design, grid integration, control and modelling. Renew Sustain Energy Rev 2022;158:112119. https://doi.org/10.1016/j.rser.2022.112119.
[13] Lebarbier CH. Power from tides - the rance tidal power station. Nav Eng J 1975;87:57–71. https://doi.org/10.1111/j.1559-3584.1975.tb03715.x.
[14] Dixon SL, Hall CA. Hydraulic turbines. Fluid mechanics and thermodynamics of turbomachinery. Elsevier; 2014. p. 361–418. 10.1016/B978-0-12-415954-9.00009-7.
[15] Michalski MAC, Melani AHA, Da Silva RF, De Souza GFM, Hamaji FH. Fault detection and diagnosis based on unsupervised machine learning methods: a Kaplan turbine case study. Energies 2021;15:80. https://doi.org/10.3390/en15010080.
[16] Zhang M, Valentín D, Valero C, Egusquiza M, Egusquiza E. Failure investigation of a Kaplan turbine blade. Eng Fail Anal 2019;97:690–700. https://doi.org/10.1016/j.engfailanal.2019.01.056.
[17] Gerini F, Vagnoni E, Seydoux M, Cherkaoui R, Paolone M. Experimental Investigation of Repurposed Kaplan Turbines as Variable-Speed Propellers for Maximizing Frequency Containment Reserve 2024.
[18] Furukawa A, Shigemitsu T, Watanabe S. Performance test and flow measurement of contra-rotating axial flow pump. J of Therm Sci 2007;16:7–13. https://doi.org/10.1007/s11630-007-0007-4.
[19] Fahlbeck J, Nilsson H, Salehi S. Surrogate based optimisation of a pump mode startup sequence for a contra-rotating pump-turbine using a genetic algorithm and computational fluid dynamics. J Storage Mater 2023;62:106902. https://doi.org/10.1016/j.est.2023.106902.
[20] Fahlbeck J, Nilsson H, Salehi S, Zangeneh M, Joseph M. Numerical analysis of an initial design of a counter-rotating pump-turbine. IOP Conf Ser: Earth Environ Sci 2021;774:012066. https://doi.org/10.1088/1755-1315/774/1/012066.
[21] Valero C, Egusquiza M, Valentin D, Presas A, Moraga G. Determination of the natural frequencies of a prototype Kaplan turbine. IOP Conf Ser: Earth Environ Sci 2022;1079:012022. https://doi.org/10.1088/1755-1315/1079/1/012022.
[22] REIVAX. Kaplan Efficiency Improvement System (Complete). REIVAX 2019. https://www.reivax.com/us/case02-automatic-full/ (accessed December 4, 2024).
[23] DIN EN 10219-1:2006-07, Kaltgefertigte geschweißte Hohlprofile für den Stahlbau aus unlegierten Baustählen und aus Feinkornbaustählen_- Teil_1: Technische Lieferbedingungen; Deutsche Fassung EN_10219-1:2006 n.d. https://doi.org/10.31030/9666332.
[24] DIN EN 10217-2:2019-08, Geschweißte Stahlrohre für Druckbeanspruchungen_- Technische Lieferbedingungen_- Teil_2: Elektrisch geschweißte Rohre aus unlegierten und legierten Stählen mit festgelegten Eigenschaften bei erhöhten Temperaturen; Deutsche Fassung EN_10217-2:2019 n.d. https://doi.org/10.31030/2524449.
[25] Hoffstaedt JP, Ruiz RA, Schürenkamp D, Jarquin-Laguna A, Goseberg N. Experimental setup and methods for a novel low-head pumped storage system. 7th Offshore Energy & Storage Symposium (OSES 2023), St. Julian's, Malta: Institution of Engineering and Technology; 2023, p. 341–8. https://doi.org/10.1049/icp.2023.1589.
[26] Truijen DPK, Hoffstaedt JP, Fahlbeck J, Jarquin-Laguna A, Nilsson H, Stockman K, et al. Hardware-in-the-loop emulator test-setup for a dual-rotor contra-rotating pump-turbine. 13th International Conference on Power Electronics, Machines and Drives (PEMD 2024), Nottingham, UK: Institution of Engineering and Technology; 2024, p. 81–8. https://doi.org/10.1049/icp.2024.2140.
[27] Gantner Instruments GmbH. Manual Q.series XL - Vers. No. 1.3 2020.
[28] Gantner Instruments GmbH. Get started with GI.bench - How To Guide 2020.
[29] dSPACE GmbH. MicroLabBox - Product Brochure 2020.
[30] dSPACE GmbH. ControlDesk v7.1 2024. https://www.dspace.com/en/inc/home/products/sw/experimentandvisualization/controldesk.cfm (accessed September 9, 2024).
[31] IEC. IEC 60193:1999 - Hydraulic turbines, storage pumps and pump-turbines - Model acceptance tests 1999. https://doi.org/ISBN number 2831849934.
[32] Dixon SL, Hall CA. Dimensional Analysis. Fluid Mechanics and Thermodynamics of Turbomachinery. Elsevier; 2014. p. 39–67. 10.1016/B978-0-12-415954-9.00002-4.
[33] Barrio R, Fernández J, Blanco E, Parrondo J, Marcos A. Performance characteristics and internal flow patterns in a reverse-running pump–turbine. Proc Inst Mech Eng C J Mech Eng Sci 2012;226:695–708. https://doi.org/10.1177/0954406211416304.
[34] Derakhshan S, Nourbakhsh A. Theoretical, numerical and experimental investigation of centrifugal pumps in reverse operation. Exp Therm Fluid Sci 2008;32:1620–7. https://doi.org/10.1016/j.expthermflusci.2008.05.004.
[35] Derakhshan S, Mohammadi B, Nourbakhsh A. Efficiency improvement of centrifugal reverse pumps. J Fluids Eng 2009;131:021103. https://doi.org/10.1115/1.3059700.
[36] de Laleu V. La Rance Tidal Power Plant 40 year operation feedback - lessons learnt. BHA Annual Conference - Liverpool 2009.
[37] Rice R, Baker G. The Annapolis Experience. OCEANS '87. Halifax, NS, Canada: IEEE; 1987. p. 391–6.
[38] Amiri K, Cervantes MJ, Mulu B. Experimental investigation of the hydraulic loads on the runner of a Kaplan turbine model and the corresponding prototype. J Hydraul Res 2015;53:452–65. https://doi.org/10.1080/00221686.2015.1040085.
[39] Alexander KV, Giddens EP, Fuller AM. Axial-flow turbines for low head microhydro systems. Renew Energy 2009;34:35–47. https://doi.org/10.1016/j.renene.2008.03.017.
[40] Jiao W, Chen H, Cheng L, Zhang B, Gu Y. Energy loss and pressure fluctuation characteristics of coastal two-way channel pumping stations under the ultra-low

head condition. Energy 2023;278:127953. https://doi.org/10.1016/j.energy.2023.127953.
[41] Aggidis GA, Feather O. Tidal range turbines and generation on the Solway Firth. Renew Energy 2012;43:9–17. https://doi.org/10.1016/j.renene.2011.11.045.
[42] Kanemoto T, Honda H, Kasahara R, Miyaji T. Operation of the counter-rotating type pump-turbine unit installed in the power stabilizing system. IOP Conf Ser: Earth Environ Sci 2014;22:012032. https://doi.org/10.1088/1755-1315/22/1/012032.
[43] Samora I, Hasmatuchi V, Münch-Alligné C, Franca MJ, Schleiss AJ, Ramos HM. Experimental characterization of a five blade tubular propeller turbine for pipe inline installation. Renew Energy 2016;95:356–66. https://doi.org/10.1016/j.renene.2016.04.023.
[44] Trivedi C, Cervantes MJ, Gandhi BK, Dahlhaug OG. Experimental and numerical studies for a high head francis turbine at several operating points. J Fluids Eng 2013;135:111102. https://doi.org/10.1115/1.4024805.
[45] Truijen DPK, Hoffstaedt JP, Fahlbeck J, Jarquin Laguna A, Nilsson H, Stockman K, et al. Impact of dual variable speed and inlet valve control on the efficiency and operating range of low-head contra-rotating pump-turbines. IEEE Access 2024;12:86854–68. https://doi.org/10.1109/ACCESS.2024.3416679.
[46] Wang H, Wang F, Wang C, Wang B, Li C, Li D. A prospective assessment of scale effects of energy conversion in ultra-low-head pumped hydro energy storage units. Energ Conver Manage 2024;315:118798. https://doi.org/10.1016/j.enconman.2024.118798.